SPATIOTEMPORAL TUNING AND CONTRAST ADAPTATION IN MOUSE PRIMARY VISUAL CORTEX

by

Emily Elizabeth LeDue

Submitted in partial fulfilment of the requirements
for the degree of Master of Science

at

Dalhousie University
Halifax, Nova Scotia
July 2012

DALHOUSIE UNIVERSITY

DEPARTMENT OF PSYCHOLOGY AND NEUROSCIENCE

The undersigned hereby certify that they have read and recommend to the Faculty of Graduate Studies for acceptance a thesis entitled "SPATIOTEMPORAL TUNING AND CONTRAST ADAPTATION IN MOUSE PRIMARY VISUAL CORTEX" by Emily Elizabeth LeDue in partial fulfilment of the requirements for the degree of Master of Science.

Dated: July 27th, 2012

Supervisor: _____

Readers: _____

_____

DALHOUSIE UNIVERSITY

DATE: July 27th, 2012

AUTHOR: Emily Elizabeth LeDue

TITLE: SPATIOTEMPORAL TUNING AND CONTRAST ADAPTATION IN MOUSE PRIMARY VISUAL CORTEX

DEPARTMENT OR SCHOOL: Department of Psychology and Neuroscience

DEGREE: MSc CONVOCATION: October YEAR: 2012

_____

Signature of Author

TABLE OF CONTENTS

LIST OF FIGURES

ABSTRACT

Mice have emerged as a popular model of cortical visual processing due to their genetic manipulability. Compared to traditional animal models of visual processing there is less research describing the visual system of mice. Before we can use the genetic techniques available in mice, we must examine the similarity between their visual processing, and that of common animal models used in vision research. One useful method to characterize the way information about form and motion is processed is to examine the interaction between selectivity for spatial and temporal frequency of sine-wave gratings in a given visual area. In experiment 1, we investigated spatiotemporal tuning in neurons of mouse primary visual cortex (V1). Tuning for stimulus speed can readily be extracted from the spatiotemporal profile of a neuron, and we were interested in whether recently described differences in the degree of speed tuning in mouse V1 and macaque V1 were due to methodology. We confirm that speed tuning is rare in mouse V1, demonstrating a difference between motion processing in the striate cortex of mice and macaques. In experiment 2, we examined the spatiotemporal dependence of contrast adaptation in mouse V1 neurons. Little is known about the underlying cellular mechanisms of contrast adaptation, so the mouse provides an attractive model in which to study this phenomenon. We characterized the spatial and temporal frequency dependence of contrast adaptation in mouse V1 neurons simultaneously using a dynamic contrast ramp. We found that for most mouse V1 neurons there was often a difference between the grating that elicited maximal firing, and the grating where adaptation was most pronounced, such that adaptation was usually stronger at higher spatial frequencies.

LIST OF ABBREVIATIONS USED

V1 primary visual cortex

RGC retinal ganglion cell

dLGN dorsal lateral geniculate nucleus

SC superior colliculus

M magnocellular

P parvocellular

K koniocellular

LM lateromedial area

LI laterointermediate area

AL anterolateral area

PM posteromedial area

MT middle temporal area

SF spatial frequency

Cpd cycles per degree

TF temporal frequency

Hz hertz

DI discrimination index

$Resp_{max}$ maximum response

$Resp_{min}$ minimum response

SSE sum of squared error

N number of presentations

M total number of different stimuli presented

F_1 first Fourier coefficient

F_0 time averaged response

K peak firing of unit

sf_0 preferred spatial frequency

tf_p preferred temporal frequency for particular spatial frequency

Q slope of relationship between preferred SF and TF

R_{insep} partial correlation between data and inseparable model

R_{sep} partial correlation between data and separable model

r_i correlation between data and inseparable model

r_s correlation between data and separable model

r_{is} correlation between inseparable and separable models

SDF spike density function

c_{50} semi-saturation contrast

Lum_{max} maximum luminance

Lum_{min} minimum luminance

ms milliseconds

$R(c_i)$ amplitude of response to a given contrast of c_i

R_{max} maximum rate of firing

R_{min} minimum rate of firing

n slope of contrast response function at the semi-saturation contrast

S spontaneous activity

ACKNOWLEDGEMENTS

Of course I could not have achieved so much alone. I would like to extend my utmost gratitude to Nathan Crowder. He has been an exceptional mentor over the last two years. I am thankful that through some unforeseen series of events I ended up with such an encouraging and sincere supervisor. I am also thankful for his endless humour late into the night and early morning of all our recording sessions.

I also must thank Aaron Stroud. Although he was gone in the final year of my degree (becoming a 'real' doctor), I am glad he was here with me to endure all the failures we had in the beginning.

Thanks to Kevin Duffy for his guidance both at the onset of my graduate studies and along the way. I also want to thank my committee members, Donald Mitchell and Steven Barnes, for all the feedback throughout this process. I am very pleased I got to meet such great faculty members.

I am extremely lucky to have the family I do. I thank my parents, John and Rita LeDue, and brother, Adam LeDue, for all their love and encouragement. I also want to especially thank my brother, Jeff LeDue, and his wife, Sarah Burke. They have truly fostered my interest in research over the last decade. Although breaking his leg was not ideal, I am glad I somehow ended up at UVic and McGill for many summers, and that I inherited such a brilliant academic woman as a sister-in-law. Their wisdom and advice have been monumentally important to me, and there is no doubt that their support and kindness has helped me get to where I am now. I could not have done it without them.

Last but not least, thank you to my fiancé Timothy O'Leary. His endurance and passion has pushed me to work harder. I am glad I found such a selfless and inspiring person to lean on during all of this, and all that is to follow.

CHAPTER 1 INTRODUCTION

1.1 Animal Models Of Human Visual Cortical Processing

Our perception of the world comes from our sensory systems, and the visual system provides us with our sense of sight. Primates are visually dominant animals that rely on vision to interpret information about the environment, and produce appropriate behavioural responses. In an attempt to parse out the complex neural calculations that govern our visual perception, and to develop and improve therapies for visual deficits, researchers make use of animal models. While human studies of visual perception are mainly limited to non-invasive psychophysical studies, animal models of vision offer a greater amount of control, manipulability, and technical options.

The primate and cat are highly visual animals and their visual systems have served as models for the study of the human visual system for the last 40 years (e.g. Hubel and Wiesel, 1963). Techniques such as neuroanatomical tracing and electrophysiological recording have allowed for the delineation of visual pathways and the functional characterization of visual areas, respectively. Cortical visual processing in these animals has been studied in depth, almost to the exclusion of other animal models. However, the argument could be made that progress in understanding cortical visual processing could be accelerated with the advent of a more genetically tractable animal model.

Mice offer the ability to genetically manipulate distinct cell types and circuits, which could aid in dissection of neural mechanisms that govern perception. Traditionally, the mouse was overlooked as a visual model because it was widely

believed that mice were not visual animals, and it was shown early on that mice had heritable retinal mutations (Keeler, 1924). Mice with normal vision have spatial acuity that is 100 times lower than that of humans, and temporal resolution about five times lower than humans (Prusky et al., 2000; Umino et al., 2010). However, early ethological observations revealed that mice show exploratory, feeding and aggressive behaviours that are both dependent on vision and visually guided (Crowcroft, 1966). Compared to cats and non-human primates, rodents are far more amicable research models and lend themselves well to life in the laboratory. Mice and rats have short generation times, reach sexual maturity quickly, and are easy to obtain and cost effective to house.

Only recently has the mouse become the subject of studies that examine normal visual processing and perception. Recent studies have revealed that the visual system of mice is both more sophisticated, and more similar to the primate visual system than originally thought (Niell and Stryker, 2008; Gao et al., 2010; Wang et al., 2010; Marshel et al., 2011; Hubermann and Niell, 2011; Wang et al., 2012). It has been shown that mice exhibit both optokinetic nystagmus and optomotor behaviours (Balkema et al., 1984; Prusky et al., 2004), and that they are capable of performing visually guided water maze tasks (Prusky et al., 2000) and forced choice touchscreen tasks (Bussey et al., 2001; Busse et al., 2011). Perhaps most importantly, transgenic mouse models are becoming a ubiquitous research tool, and this genetic technology is not yet feasible in cats and primates. The newfound use of mice in studies of normal visual processing, in combination with transgenic modifications, makes mice an attractive animal model of human cortical

visual processing and development. These transgenic modifications have drastically increased the use of the mouse visual system in studies of cortical plasticity (Zhang et al., 2007; Luo et al., 2008). However, in order to assess the relevance of conclusions drawn from these studies using mouse primary visual cortex (V1), the similarity of the basic properties of mouse V1 to that of higher mammals needs to be evaluated.

1.2 Introduction To Geniculostriate Pathway Of Mammals

The geniculostriate pathway is the most commonly studied visual pathway, and its plasticity and normal function has most often been linked with visual perception (Van Essen, 1979; Carandini et al., 1999). In the first section below, the geniculostriate pathway of macaques will be briefly described. Macaques are the dominant primate model of human visual processing and their geniculostriate pathway is highly homologous to that of humans. The second section will focus on the geniculostriate pathway of mice and emphasize similarities and differences between the macaque and mouse pathways.

1.2.1 Macaque Visual Pathway To V1

The basic components of the macaque geniculostriate (or retinothalamocortical) pathway include the eye, thalamic relay structures and visual cortical areas. Macaques, like humans, have forward facing eyes that are highly mobile (Fuchs, 1967; Schall et al., 1995). Light coming into the eye reaches the retina, which contains two types of photoreceptors: rods and cones. Although the total number of rods far exceeds that of cones, in macaque retina, cones are concentrated in a central region called the fovea and reach an average peak density

of around 210000/mm^2 (Packer et al., 1989). Rods and cones allow for vision in dim, (scotopic) and bright (photopic) lighting conditions, respectively. Cones can be classified based on their peak wavelengths, of which there are three main types: long (565 nm), medium (530 nm) and short (420 nm) (Kiper et al., 1997; Calkins and Sterling, 1999; Nathans, 1999). In terms of visual function, cones provide fine spatial resolution of the visual field, which is known as visual acuity, and also trichromatic vision in macaques (Wikler et al., 1990; Rowe, 2002). The visual image is further processed by retinal circuitry, and the visual signal exits the eye through the axons of retinal ganglion cells (RGC). In primates a subpopulation of these axons project directly to the dorsal lateral geniculate nucleus (dLGN) of the thalamus, which is retinotopically organized. A smaller portion of retinal ganglion axons also project to other relay structures such as the superior colliculus (SC), hypothalamus, and pretectum to form the other retino-recipient pathways (Perry and Cowey, 1984).

The primary visual cortex (V1) is responsible for many transforms of visual coding, and the stimulus features that drive the responses of V1 neurons are well established. In macaques, V1 receives dLGN input from three principal cell types: koniocellular (K), magnocellular (M) and parvocellular (P). V1 itself consists of six retinotopically organized layers. Layer 1 consists of mainly white matter, and collectively, layers 2/3 and layers 5/6 are known as the supragranular and infragranular layers, respectively. Layer 4 has a preponderance of simple cells and is the main input layer of V1, receiving highly ordered and intricate projections. Layer 4 is further subdivided into layer 4A, 4B, 4Cα, and 4Cβ, which are collectively known

as the granular layers (Callaway, 1998). Layers 4Cα, and 4Cβ receive input from primarily M and P cells, respectively. The infragranular layers send feedback to the dLGN and the SC. Superficial layer 4B and the supragranular layers send output to other cortical regions, forming cortico-cortical connections. M and P/K cell projections form distinct streams of processing that project to extrastriate regions, and these connections have been extensively mapped (Sincich and Horton, 2002a,b; 2003). P/K and M cells appear to project to particular extrastriate locations and, in general, these two streams are referred to as the dorsal and ventral pathways. The dorsal stream processes the spatial location of objects, object motion, and self-motion, whereas the ventral pathway is involved in object recognition and color vision (Goodale and Milner, 1992; Andersen, 1997; Britten and Van Wezel, 2002; Conway et al., 2010; Maunsell and Van Essen, 1987; Britten et al., 1992).

1.2.2 Mouse Visual Pathway To V1

Mice have laterally positioned eyes that have a range of motion of only about two degrees of visual angle (Métin et al., 1988; Andermann et al., 2011). Similar to the macaque, the mouse retina consists primarily of rods, with cones comprising only 3% of the total photoreceptor population (Porciatti et al., 1999; Wang et al., 2011). The mouse lacks a fovea, but there is a minor increase in peak density of cones at the area centralis, which reaches about 12400/mm^2 (Jeon et al., 1998). In fact, although the total percentage of cones in primate retina far exceeds that found in the mouse, it appears that the average density of rods and cones in the mouse retina is similar in magnitude to the average densities found in the periphery of the macaque retina (Packer et al., 1989; Wikler and Rakic, 1990). The mouse retina has

two types of cones, which are sensitive to wavelengths of around 360 and 510 nm (Haverkamp et al., 2005). The remainders of the retinal cell populations (bipolar cells, horizontal cells, etc.) of the mouse are essentially similar to that of macaque (Jeon et al., 1998), and retinal axons converge on RGCs before leaving the eye. These RGCs make projections to similar regions as in primates, such as the SC and dLGN of the thalamus (Dräger and Olsen 1980). Like in primates, the mouse dLGN receives direct retinal ganglion cell projections and then projects to V1, which is the only cortical region of the mouse that is principally innervated by the dLGN (Figure 1; Valverde, 1991; Rodieck and Watanabe, 1993). The architecture of mouse V1 is also similar to primates; it is comprised of 6 layers, each of which receives topographically organized input in order to create a complete spatial representation of the contralateral visual hemifield (Wagor et al., 1980; Schuett et al., 2002; Kalatsky and Stryker, 2003), and includes both monocular and binocular regions (Dräger, 1975, 1978; Wagor et al., 1980; Gordon and Stryker, 1996). Cortical layers of mouse V1 are organized in the same way as was described for macaque V1, with layer 4 being the main input layer (Wang and Burkhalter, 2007; Wang et al., 2011). Recently several distinct extrastriate areas, receiving the majority of their inputs from V1, have also been described in the mouse (Wang and Burkhalter, 2007; Andermann et al., 2011; Marshel et al., 2011).

Interestingly, many extrastriate areas in mouse appear to be homologous to those found in the primate (Andermann et al., 2011). The lateromedial area (LM)

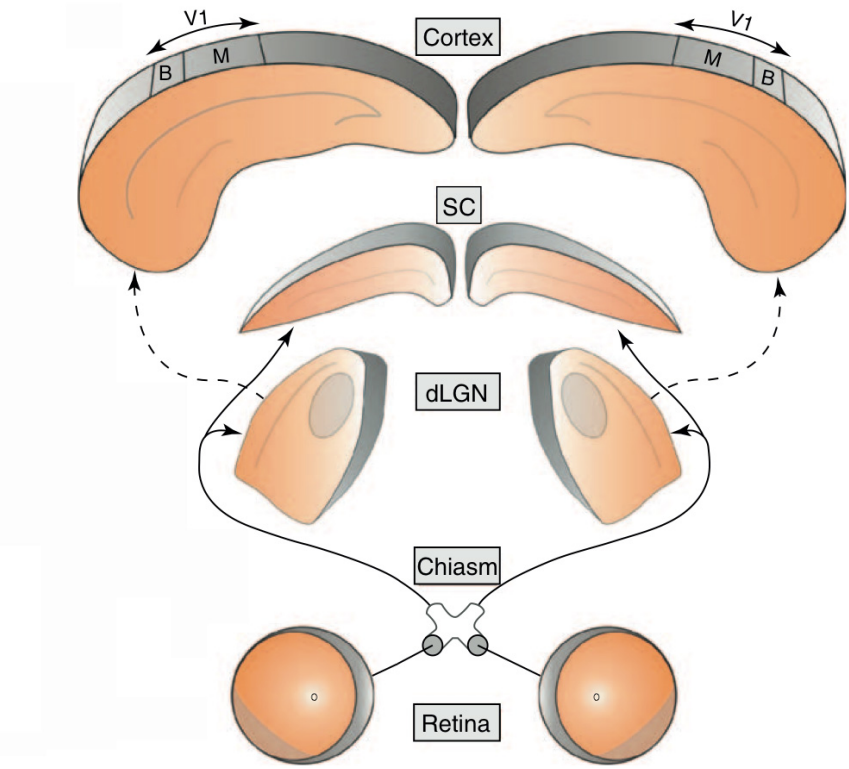

Figure 1. Diagram of the mouse visual pathway. Direct retinal projections to both the dorsal lateral geniculate nucleus (dLGN) and the superior colliculus are indicated by the solid arrows. The dashed arrows represent the geniculocortical pathway projection from the dLGN to the primary visual cortex. B and M denote the small binocular and larger monocular regions of the primary visual cortex, respectively (Adapted from Huberman and Niell, 2011).

has been proposed as the mouse homologue of primate V2 (Wang and Burkhalter, 2007; Andermann et al., 2011). Similarly, it has been suggested that mouse laterointermediate area (LI) may be the homologue of primate V3 (Wagor et al., 1980; Wang and Burkhalter, 2007). Both areas LM and LI appear to contain topographic representations of different parts of the contralateral visual field that, when integrated, form another complete representation of the contralateral visual hemifield (Wagor et al., 1980). Mouse V1 neurons also project to other retinotopically organized extrastriate areas such as: the anterolateral area (AL) and the posteromedial area (PM) (Figure 2; Wang and Burkhalter, 2007; Andermann et al., 2011; Marshel et al., 2011). The majority of functional information inferred about these regions has come from lesion studies (Prusky and Douglas, 2004; Prusky et al., 2008) and studies examining anatomical connectivity and location respective to V1 (Wang et al., 2011). Specifically, it has been proposed that areas LM and AL might resemble the areas that make up the primate ventral and dorsal stream, respectively (Wang et al., 2011). Mouse area PM is thought to be homologous to the middle temporal (MT) area in the primate area, which is a well-studied cortical area associated with processing visual stimulus motion (Zemel and Sejnowski, 1998; Lui et al., 2006).

1.3 Physiology Of Primary Visual Cortex Neurons

Though the visual system of mice is similar to that of primates in many ways, as mentioned previously mice have dichromatic vision and laterally placed eyes, which implies they do not make use of color or stereoscopic depth cues as macaques do. Therefore, we will focus on the common properties that drive the responses of

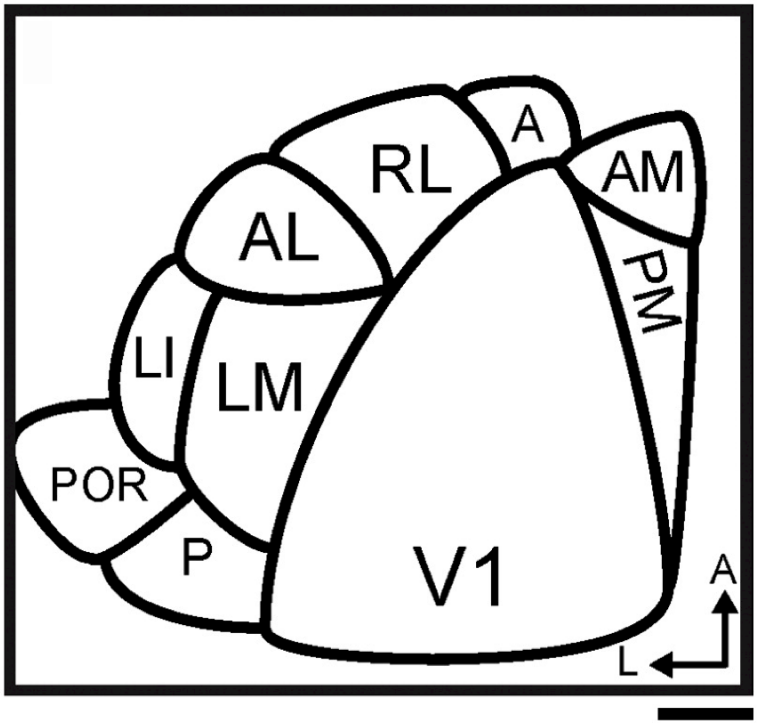

Figure 2. Diagram of mouse visual cortex showing area borders between regions. The primary visual cortex (V1) makes direct projections to extrastriate areas such as the anterolateral area (AL) and the posteromedial area (PM). Arrows indicate the anterior and lateral directions. Scale bar represents 500 μm (Adapted from Marshel et al., 2011).

V1 neurons in both species: 1) orientation, 2) spatial and temporal frequency tuning, and 3) image contrast.

1.3.1 Orientation

V1 neurons respond preferentially to stimuli with edges or contours that extend along certain orientations. A neuron's preferred orientation will produce maximum firing relative to other orientations. Orientations that fall between the preferred and orthogonal orientation (40 - 90° away from preferred) will elicit progressively less firing (Hubel and Wiesel, 1968). In the macaque about 87% of neurons show selection for orientation (Hubel and Wiesel, 1974; Schiller et al., 1976; Hubel et al., 1978). In addition, there are some cells that respond maximally to motion along a single direction.

There are two principal cell types within V1: simple cells and complex cells. These cell types were described in macaque by Hubel and Wiesel (1968) and later in the mouse (Niell and Stryker, 2008). Simple cells appear to be created from the linear summation of multiple center surround dLGN inputs and possess distinct, spatially segregated ON and OFF regions (Reid and Alonso, 1995). ON regions are excited by increments in luminance and inhibited by decrements in luminance, while OFF regions are excited by decrements in luminance and inhibited by increments in luminance (Ferster, 1988). Simple cells are sensitive to the phase (position) of a grating stimulus, and respond maximally when the orientation of a light and dark bar matches the positioning of their ON and OFF subregions, respectively (DeAngelis et al., 1993; Wielaard et al., 2001). It is proposed that inputs to a simple cell are organized as a *push-pull* mechanism. An ON subregion of a

simple cell can be created by the combination of excitatory inputs from an ON-center cell and inhibitory inputs from an OFF-center cell (Tolhurst and Dean, 1987). The *push-pull* mechanism has been described in precortical LGN cells with center surround receptive fields and in neurons of cortical visual areas (Hubel and Wiesel, 1962). The receptive fields of complex cells are spatially homogenous and do not possess segregated ON and OFF regions, and can be described by a *push-push* mechanism (Martinez et al., 2005). Unlike simple cells, the position of the stimulus within the receptive field does not dictate the cell's responsiveness. Regardless, complex cells also show a preference for particular orientations.

Mouse V1 neurons are noted for having broad ranges of orientation tuning, and truly direction selective cells are more rare in mouse V1 than in primate V1 (Mangini and Pearlman, 1980; Livingstone, 1998; Niell and Stryker, 2008). In mouse V1, about 40% of neurons were shown to have some degree of orientation selectivity (Dräger, 1975; Mangini and Pearlman, 1980; Métin et al., 1988), with some neurons showing no preference for particular orientations, while some neurons show complete selectivity (Niell and Stryker, 2008).

1.3.2 Spatial And Temporal Frequency

In studies of the visual system, the longstanding stimulus of choice has been the sine wave grating because its luminance shift over space and time can be described by a sinusoidal function (Enroth-Cugell and Robson, 1984). For sine wave gratings, the spatial frequency (SF) of a stimulus is described as the number of cycles that are subtended by one degree of visual angle at the eye and is measured in cycles per degree (cpd). The temporal frequency (TF) of a sine wave grating

describes how many cycles are generated per unit of time and is measured in cycles per second or hertz (Hz). Tuning functions for SF and TF have been well characterized independently in both macaque and mouse V1 neurons (De Valois et al., 1982; Foster et al., 1985; Hawken et al., 1996; Neill and Stryker 2008; Gao et al., 2010).

In macaque, visual acuity threshold reaches about 38 cpd at the fovea (Merigan and Katz, 1990). Electrophysiological studies of V1 neurons in macaque report preferred spatial and temporal frequencies ranging from 1.9 to 3 cpd and 7.8 to 8 Hz, respectively (Foster et al., 1985; Bair and Movshon, 2004). Compared to macaques, mice have far poorer visual acuity, with an acuity threshold of about 0.5 cpd (Prusky et al., 2000). Despite their low visual acuity, mouse V1 neurons still show robust SF and TF tuning (Niell and Stryker, 2008; Gao et al., 2010; Andermann et al., 2011; Marshel et al., 2011). Niell and Stryker (2008) reported that most mouse V1 neurons preferred SFs between 0.02 and 0.08 cpd, with a median preferred SF of 0.036 cpd. Similar results were found by Gao et al. (2010), where neurons recorded in V1 preferred SFs ranging from 0.02 – 0.09 cpd, with the median preferred SF of 0.03 cpd. Marshel et al. (2010) used two-photon *in vivo* calcium imaging to measure tuning properties in anesthetized mouse V1 and reported a mean preferred SF of 0.045 cpd in V1 neurons, which is similar to the values obtained through electrophysiological recordings (Niell and Stryker, 2008; Gao et al., 2010).

Gao et al. (2010) determined that mouse V1 neurons had median preferred TFs of between 1.2 - 1.9 Hz. Niell and Stryker (2008) reported mouse V1 neurons as

having a median preferred TF of 1.68 Hz, which falls within the range reported by Gao et al (2010). Marshel et al. (2010) reported a preferred TF of 0.69 Hz in V1 neurons, but the differences between the preferred TF values reported by Marshel et al. (2010) may stem from differences between single-unit electrophysiological recordings and calcium imaging.

1.3.2 Image Contrast And Contrast Adaptation

Contrast is defined as the difference between the maximum and minimum luminance of a stimulus across space. A contrast of 1 indicates that there is a maximal difference between the minimum and maximum luminance of a stimulus, while a contrast of 0 represents a homogenous grey. It appears that all visual neurons derived from inputs that possess ON and OFF regions (the *push-pull* mechanism described previously) code for stimulus contrast. In V1 neurons, response to a sine wave grating increases when the contrast of the grating is increased and the neural response to contrast can be described by a sigmoidal function (Ohzawa et al., 1982). The center range of this response function describes the contrast range to which the neuron is most sensitive (i.e., firing rate changes with contrast).

When discussing the visual system, the term adaptation refers to when recent sensory experience changes a neuron's response properties in order to adjust for current conditions (Kohn, 2007). Adaptation to stimulus contrast was first reported as a perceptual phenomenon in psychophysical studies after exposure to an adapting stimulus of high spatial contrast. The perceived contrast of a post-adaptation test stimulus was reduced compared to pre-adaptation measures, and

contrast sensitivity was also decreased (Blakemore and Campbell, 1969; Blakemore et al., 1973). At the neuronal level, adaptation is characterized by a rightward and downward shift in the typical sigmoidal contrast response function of V1 neurons, which are called contrast gain control and response gain control, respectively (Bonds, 1991; Carandini and Ferster, 1997). The characteristics of contrast adaptation have been studied extensively, but mechanisms underlying this phenomenon are unclear. In V1, both complex and simple cells show contrast adaptation, and one proposed functional benefit of adaptation is that it allows neurons to maintain stimulus discriminability by shifting their response function to higher contrasts after being exposed to a high contrast adaptor (Kohn, 2007). It has been reported that contrast adaptation is dependent upon the spatial and temporal frequency of the adaptor, and maximum adaptation occurs when the SF and TF of the adapting grating is similar to the SF and TF of the test grating (Movshon and Lennie, 1979; Saul and Cynader, 1989).

1.4 Objective Of The Current Experiments

In order to determine the suitability of using the mouse as an animal model of cortical visual processing, we sought to examine the interaction between SF and TF tuning in mouse V1, as well as how these stimulus parameters affected contrast adaptation. The interaction between SF and TF tuning is important because the ratio of TF and SF of a sine wave grating defines its speed, and stimulus speed is a biologically relevant parameter for many species. In addition, TF and SF affect the firing rate of a neuron, which has been previously linked to contrast adaptation. However, the effects of TF and SF on adaptation have been assessed separately in

the past, and the current work is the first instance where the influence of both factors has been assessed together. Characterizing the interaction between SF and TF in driving neural responses is an important step in understanding how the mouse visual system codes stationary and moving images.

1.4.1 Experiment 1

As mentioned previously, the ratio of the temporal and spatial frequency of a sine wave grating defines its speed. In macaques, studies have characterized the neuronal response to moving sine wave gratings in both V1 and area MT, which can be classified as separable or inseparable. Inseparable neurons have a constant preferred speed over a range of SFs, while separable neurons show a preference for a particular SF and their preferred speed varies with TF (Perrone and Thiele, 2001; Priebe et al., 2003; Priebe et al., 2006). In macaque, it is reported that around 25 – 60% of neurons in MT and 25% of V1 complex neurons are speed selective (Perrone and Thiele, 2001; Priebe et al., 2003; Priebe et al., 2006). Recently, Andermann et al. (2011) examined speed tuning in mouse V1 using *in vivo* calcium imaging and found that speed tuned neurons were rare among the population and as a whole, V1 was not speed selective.

In experiment 1, we sought to characterize the spatiotemporal tuning profile of mouse V1 neurons by using single unit *in vivo* electrophysiology. We were interested in whether recently described discrepancies seen in the spatiotemporal tuning properties of macaque V1 neurons and mouse V1 neurons were due to methodological differences, as studies in macaque have used *in vivo* electrophysiology, and the recent study in mouse V1 used *in vivo* calcium imaging

(Priebe et al., 2003; Andermann et al., 2011). We tested single units in mouse V1 with drifting sine wave gratings of varying spatial and temporal frequency combinations in order to measure the response of a single neuron as a function of both spatial and temporal frequency.

1.4.2 Experiment 2

In experiment 2, we asked whether the SF and TF that elicited maximum firing (preferred SF and TF of the neuron) also produced maximum contrast adaptation. It is well known that contrast adaptation is dependent upon both the spatial and temporal frequency of the adaptor (Movshon and Lennie, 1979; Maddess et al., 1988; Saul and Cynader, 1989a). In particular, for V1 neurons, contrast gain control appears to be SF specific, and is seen only when the SF of the adaptor and the test stimulus are comparable (Movshon and Lennie, 1979). Saul and Cynader (1989a) showed that maximum adaptation occurred at the preferred SF and TF of the neuron, when tested with stimuli that were similar to the adaptor. In experiment 2, we adapted and tested mouse V1 neurons at different spatiotemporal frequencies in order to measure contrast adaptation at each unique combination. We were interested in whether contrast adaptation in mouse V1 neurons was also dependent on the SF and TF of the adaptor, as shown in macaque and cat. In addition, we covaried SF and TF together in order to measure responses from single units to both parameters simultaneously, which has never been done in any species.

CHAPTER 2 SPATIOTEMPORAL TUNING IN MOUSE V1[1]

2.1 INTRODUCTION

Visual motion is a salient and biologically relevant visual stimulus for many animals (Albright and Stoner, 1995; Giese and Poggio, 2003). In behavioural tasks, human and non-human primates are capable of extracting the speed of a moving stimulus from the visual array (Lisberger et al., 1987; Bair and O'Keefe, 1998; Born and Bradley, 2005; Schlack et al., 2008), and humans are capable of discerning variations in stimulus speed of < 5% (McKee, 1986). Any moving visual stimulus can be decomposed into sine wave gratings of various spatial frequencies (SF) and temporal frequencies (TF), and the neural processing of stimulus speed can be tested in the laboratory using drifting sinusoidal gratings as simplified stimuli because a grating's speed is calculated as the ratio of its TF and SF. In macaques, studies in early visual cortex and specialized motion processing areas like the middle temporal area (MT) have revealed that neuronal responses to these sine wave stimuli can be classified as either inseparable or separable: inseparable neurons have a constant preferred speed over many SFs, but separable neurons have a preferred SF and their preferred speed varies with TF (Perrone and Thiele, 2001; Priebe et al., 2003; Priebe et al., 2006). Around 25-60% of MT neurons, and 25% of V1 complex neurons have been found to be speed selective in macaques (Perrone and Thiele, 2001; Priebe et al., 2003; Priebe et al., 2006).

Behavioural studies have shown that mice, like primates, are sensitive to stimulus speed (Umino et al., 2010). Recently, mice have become a popular model of

[1] A version of this chapter has been submitted to Neuroscience Letters

cortical visual processing because of the availability of genetic tools that allow for manipulation of different cell types or circuits that are important for vision. Despite the poor visual acuity of the mouse, their V1 shares many similarities with primates, such as SF tuning, orientation tuning, and the presence of both simple and complex cells (Niell and Stryker, 2008; Gao et al., 2010). The small size and lissencephalic structure of the mouse cortex could also be viewed as advantageous, as it allows easy simultaneous study of striate and extrastriate visual areas using electrophysiology or imaging techniques. It is possible that mouse models could provide us with insight into the neural processing of motion coding and speed tuning, but comparisons to existing research in other species must first be established.

Andermann et al. (2011) were the first to investigate speed tuning in mouse striate and extrastriate areas using *in vivo* two-photon calcium imaging in awake animals and found that unlike macaque V1, very few neurons in mouse V1 were speed selective, and that other extrastriate areas were responsible for processing of stimulus speed. Although calcium imaging allows data collection from huge populations of individual neurons simultaneously, it is an indirect measure of spiking rate, so there are several caveats in interpreting this data. First, the fluorescence of both synthetic and genetically coded calcium indicators is non-linear, and saturation creates difficulty in interpreting very high or low spike rates (Tian et al., 2009), although the GCAMP3 indicator used by Andermann et al. (2011) suffers less from these problems. Second, calcium imaging is currently limited to the superficial layers of the cortex. We were interested in whether the difference

between macaque V1 and mouse V1 neurons might be due to methodological differences, as speed tuning in macaque V1 was measured using electrophysiology in anesthetized animals.

In this study, we recorded single-unit responses in anesthetized mice to drifting sine wave gratings for 36 combinations of SFs and TFs to obtain spatiotemporal response profiles. To evaluate the magnitude of speed tuning for each unit we fit our data with a two-dimensional Gaussian following the methods used in macaque studies (Priebe et al., 2003), and calcium imaging studies in mouse (Andermann et al., 2011). Our results were also re-analyzed with a partial correlation analysis following Priebe et al. (2003). We found that inseparable tuning was rare in mouse V1, which agrees with earlier data obtained with two-photon calcium imaging (Andermann et al., 2011).

2.2 Materials And Methods

2.2.1 Animals

Experiments were performed on 17 adult male C57BL/6J weighing between 20 and 30 grams (Purchased from Jackson Laboratories). The University Committee on Laboratory Animals approved all experimental procedures.

2.2.2 Surgical And Physiological Preparation

Mice were anesthetized with urethane (1.2g/kg ip, Sigma Aldrich, St. Louis, MO) and body temperature was maintained at 37.5°C with a heating pad. If needed, a small dose of ketamine (20mg/kg ip) was given to accelerate descent to the surgical plane of anesthesia (Moldestad et al., 2009). A tracheotomy was performed prior to securing mice in a stereotax (Moldestad et al., 2009). Mice were left free

breathing throughout the experiment and a tube located in front of the mouse delivered oxygen (0.1 L/min) to supplement room air. Additional urethane doses were given as required, and chlorprothixene (5mg/kg ip, Sigma Aldrich) was also given with the first urethane top up. A craniotomy (~1mm^2) was made 0.8 mm anterior and 2.3 mm lateral to lambda (Paxinos and Franklin, 2001), which corresponds to the primary visual cortex in mice. Recordings were made using either glass (2-5µm tip diameter, filled with 2M NaCl) or carbon fiber in glass microelectrodes (0.6 - 1.5MΩ impedance). Electrode depth was controlled using a micromanipulator (FHC, Bowdoin, ME). Extracellular signals from individual units were amplified and filtered (FHC) before being digitized (Cambridge Electronic Design Power1401 with Spike2, Cambridge, England). Acquired signals were sampled at 40kHz, and online analysis was performed on triggered TTL pulses with Spike2, but subsequent analysis was done offline.

2.2.3 Visual Stimuli

Receptive field locations for visually responsive units were initially mapped out by hand using a light bar, then quantitatively characterized online for orientation selectivity and surround suppression using drifting square wave gratings. Spatiotemporal tuning was assessed with drifting sine wave gratings with 36 combinations of SFs (0.01, 0.02, 0.04, 0.08, 0.16 and 0.32 cpd) and TFs (0.25, 0.5, 1, 2, 4, 8 Hz). All spatiotemporal stimuli were presented at the optimal orientation and size for each unit. Presentations of different spatiotemporal combinations were randomized with 8 – 10 repeats for each combination. The presentation time of the stimulus was 1.5 seconds, and a grey of mean luminance was shown between

stimuli for 0.5 seconds. Grating start-phase was staggered on each repetition to average out periodic firing of phase-sensitive neurons. Viewing distance depended on the location of the receptive field and was adjusted on a unit-to-unit basis, but ranged from a distance of 15 to 35 cm. All units were from the monocular representation of V1 (~30 – 100° lateral to the vertical meridian; Paxinos and Franklin 2001; Schuett et al., 2002). All stimuli were custom made using the Psychophysics toolbox extension for Matlab (Mathworks, Natick MA; Brainard 1997; Pelli 1997) and presented on a calibrated CRT monitor (LG Flatron 915FT plus 19", 100Hz refresh rate, 1024x768 pixels, mean luminance = 30 cd/m^2).

2.2.4 Initial Data Analysis

2.2.4.1 Strength of Tuning for Orientation and Patch Size

Spike sorting was performed with Spike2 (Cambridge Electronic Design) and a principle components analysis was used to isolate single units. For each unit, we calculated the magnitude of orientation and size tuning using a discrimination index (DI) (DeAngelis and Uka, 2003):

$$\text{Discrimination Index} = \frac{(Resp_{Max} - Resp_{Min})}{((Resp_{Max} + Resp_{Min}) + 2\sqrt{SSE}/(N-M))} \quad (1)$$

$Resp_{Max}$ is the neuron's max response, while $Resp_{Min}$ is the neuron's minimum response. SSE is the sum of squared error of the mean, N is the total number of presentations of the stimuli, and M is the number of different stimuli presented.

2.2.4.2 Spatial Summation

In order to classify cells as simple or complex, we divided the first Fourier coefficient of a neuron's response to a grating at the spatiotemporal peak (F_1) by the mean time-averaged response to this grating (F_0). The F_1/F_0 ratio has been used to

quantitatively classify simple and complex cells (Schiller et al., 1976; Skottun et al., 1991; Movshon et al., 1978a,b), and an F_1/F_0 ratio less than 1 indicates a cell is complex.

2.2.4.3 Spatiotemporal Tuning And Two Dimensional Gaussian Fits

In order to quantify speed tuning in individual neurons we fit spatiotemporal responses to a two-dimensional Gaussian using the least squares method (following the fitting methods used by Priebe et al., 2003, and also by Andermann et al., 2011):

$$R(sf, tf) = K * exp\frac{-(log_2(sf)-log_2(sf_0))^2}{\sigma_{sf^2}} * exp\frac{-(log_2(tf)-log_2(tf_p(sf)))^2}{\sigma_{tf^2}} \quad (2)$$

where K is the peak response, sf_0 is the neuron's preferred spatial frequency and tf_p is dependent on the preferred spatial frequency, as defined by:

$$tf_p(sf) = 2^{(Q+1)*log_2(sf)-log_2(sf_0))+log_2(tf_0)} \quad (3)$$

The parameter Q defines the slope of the relationship between the preferred TF and SF. If a neuron is inseparable, its preferred speed will remain constant as the SF of the stimulus is altered, and Q will be around 0. In contrast, if a neuron is separable, its preferred speed changes as SF changes, and Q will be approximately -1. A secondary analysis which also addressed speed tuning used partial correlations to test whether a neuron's tuning was more highly correlated with a model in which Q was constrained to either -1 or 0, which represented complete separability or perfect speed tuning, respectively. Partial correlations were calculated using the following equations (Priebe et al., 2003):

$$R_{insep} = \frac{(r_i - r_s * r_{is})}{\sqrt{(1-r_s^2)(1-r_{is}^2)}} \quad (4)$$

$$R_{sep} = \frac{(r_s - r_i * r_{is})}{\sqrt{(1 - r_i^2)(1 - r_{is}^2)}} \quad (5)$$

where R_{insep} and R_{sep} are the partial correlations between the data and an inseparable and separable model, respectively. The values r_i, r_s and r_{is} represent the correlation between the data and the inseparable model, the data and the separable model, and the two models, respectively.

2.3 Results

We recorded visual responses from 176 units in the primary visual cortex of 17 C57BL/6J mice, of which full spatiotemporal data sets were obtained from 146 units. Because we used online tuning functions to optimize our stimuli to the response properties of each neuron we were able to compare the general stimulus preferences of neurons in our sample with previous studies.

2.3.1 Discrimination Index For Orientation And Size

Our sample of V1 neurons had a median orientation DI of 0.49, which is similar to other studies (Neill and Stryker, 2008; Gao et al., 2010). True orientation selective cells were defined as having a 2:1 modulation of firing in response to orientations that elicited maximum and minimum responses, respectively. Cells that had a 2:1 modulation or better had corresponding orientation DIs of 0.53, on average. In our data set, we found that 48% of neurons (70/146) showed 2:1 modulation or better and these neurons were deemed to be orientation selective. The median DI for patch size for our population of V1 neurons was 0.59. A one-way ANOVA was used to determine whether neurons showed significant surround

suppression ($p < 0.05$). We found that only 9 units showed significant surround suppression with the patch sizes we tested (maximum = 64°).

2.3.2 Spatial Summation

Since it has been shown that only complex cells in macaque V1 possess speed tuning (Priebe et al., 2006), we quantitatively categorized our neurons as either simple or complex using F_1/F_0 ratios. We found that the majority of cells, 92% (134/146), had an F_1/F_0 ratio < 1 and were therefore classified as complex. Similar to Gao et al. (2010) simple cells were rare among the population, comprising only about 8% of the total number of units (12/146). The population average F_1/F_0 ratio in our sample was 0.53 ± 0.34 (mean ± SD).

2.3.3 Spatiotemporal Tuning

Figure 3A shows the spatiotemporal profile of a representative neuron, with a spike density function (SDF) for each of the 36 combinations of spatial frequency and temporal frequency. This neuron prefers SFs of around 0.02 cpd and TFs of around 4 Hz. When the mean response to each combination was summarized as a contour plot (Figure 3B), the location of the peak is easily seen. Peak SFs and TFs were broadly distributed, with preferred SFs ranging from 0.01 to 0.17 cpd and preferred TFs ranging from 0.25 to 8 Hz. The average preferred SF and TF for our population of neurons was 0.03 cpd and 1.72 Hz, respectively. Contour plots were then fit to two-dimensional Gaussians and the goodness of fit for each unit was assessed with using r^2 (Figure 3C). Units with multiple spatiotemporal peaks were

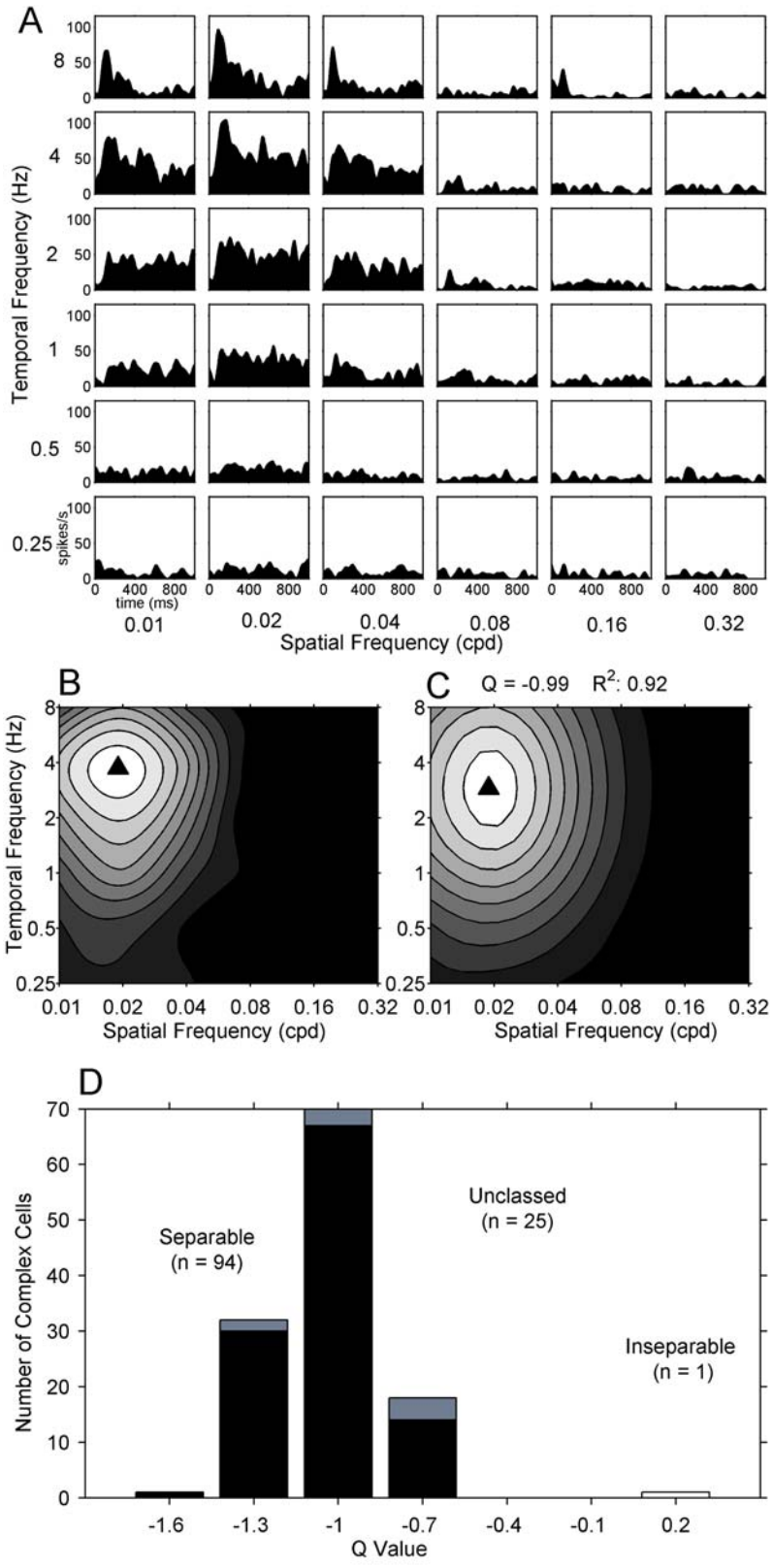
A
Temporal Frequency (Hz)
8
4
2
1
0.5
0.25
100
50
0
spikes/s
0
400
800
time (ms)
0.01
0.02
0.04
0.08
0.16
0.32
Spatial Frequency (cpd)
B
C
Q = -0.99
R2: 0.92
Temporal Frequency (Hz)
Spatial Frequency (cpd)
D
Number of Complex Cells
Separable
(n = 94)
Unclassed
(n = 25)
Inseparable
(n = 1)
-1.6
-1.3
-1
-0.7
-0.4
-0.1
0.2
Q Value

Figure 3. Spatiotemporal tuning of mouse V1 neurons. A shows the spatiotemporal profile of a sample neuron, where the response to each combination of SF and TF is shown as a SDF. The mean data from A is summarized as a contour plot (B). Contour plots were fit to a two-dimensional Gaussian (C) and the goodness of fit was assessed using r^2 (0.92 for this neuron, $p < 0.0001$). In each contour plot, the peak preferred spatiotemporal frequency is indicated by a closed triangle. The magnitude of speed tuning across the population, as measured by the fit parameter Q, is summarized as a histogram (D). The black, white and grey bars represent complex cells whose 95% confidence interval around Q overlapped with -1 (separable), overlapped with 0 (inseparable), or were between 0 and -1 (unclassed), respectively. It is clear that most neurons in our population were classified as separable.

poorly fit by a two-dimensional Gaussian (n = 17), and were therefore excluded from subsequent analysis. Fits were quite good for the remaining cells (n = 129, mean $r^2 = 0.8$)

For neurons that could be adequately fit to the two-dimensional Gaussian, we then used the parameter Q to measure the degree of speed tuning. Similar to previous studies, we used the 95% confidence interval around the Q value for each unit in order to classify neurons as separable, inseparable or unclassed (Priebe et al., 2003; Priebe et al., 2006; Lui et al., 2007). For the majority of complex units in our sample (112/122) the confidence interval around Q was inclusive of -1, and these units were classified as separable (Figure 3D black bars). Only 1 complex cell had a 95% confidence interval that overlapped with 0 and was therefore classified as inseparable (Figure 3D, white bar). The remainder of complex cells, 9/122, did not fall in either category and were therefore unclassed (Figure 3D, grey bars). All simple cells in our sample had a 95% confidence interval around Q that included -1 and were classified as separable (n = 7). The mean Q value of the population of V1 simple and complex neurons in our sample was -1.01 (standard deviation = 0.25, n = 129), which is similar to Andermann et al. (2011). There was no significant difference between Q values of simple and complex cells in our sample (Wilcoxon rank sum test, p = 0.12).

As a secondary analysis we examined the speed tuning of our sample using the partial correlation method of Priebe et al. (2003). We correlated the spatiotemporal contour plot for each unit with two models: i) the separable model, where Q was constrained at -1; and ii) the inseparable model where Q was

constrained at 0. Three complex neurons from our sample were removed at this stage of analysis because they could not be fit to the constrained inseparable model. Real data from a representative neuron (Figure 4A) is shown alongside its separable (Figure 4B) and inseparable fits (Figure 4B). For this neuron, the r^2 values for separable and inseparable fits were 0.92 and 0.84, respectively. Partial correlations were plotted as a scatter plot, with solid and open circles representing simple and complex cells, respectively (Figure 4D). Out of our remaining 119 complex units, we found 25 were unclassed and 94 showed tuning closely resembling the independent predictions. Simple cells showed a similar classification to complex cells, with 4/7 being classified as separable and the remainder was unclassed (3/7). Classifications based on partial correlation analysis and Q were quite similar, but the single speed tuned neuron as classified with the 95% confidence interval around Q was unclassed using partial correlations. This neuron did lie close to the significance line for speed tuning, as represented by the cross in figure 4D.

2.4 Discussion

In this study we measured spatiotemporal tuning in mouse V1 neurons using single unit *in vivo* electrophysiology, which complemented recent findings using two photon *in vivo* calcium imaging (Andermann et al., 2011). Both studies found that very few neurons in mouse V1 were speed tuned, and the average Q value for V1 neurons in our study is similar to that reported by Andermann et al. (2011). This provides evidence that the scarcity of speed tuned neurons originally reported for mouse V1, compared to macaque V1, was not due to technical differences. These

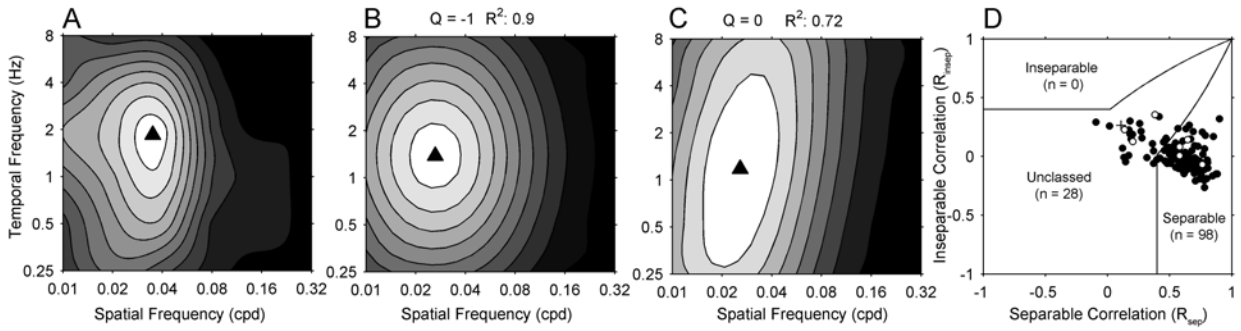

Figure 4. Partial correlation analysis. The spatiotemporal contour plot of a representative neuron (A) was correlated with two models: the separable model in which Q was constrained at -1 (B), and the inseparable model in which Q was constrained at 0 (C). The peak spatiotemporal frequency is represented by a closed triangle. Partial correlations for the population of neurons (n = 129) are shown as a scatter plot (D). Filled and open symbols represent complex and simple cells, respectively. The single neuron that had a 95% confidence interval around Q that overlapped with 0 in Figure 3 is shown as a cross. Solid lines represent the division of separable, inseparable and unclassed neurons.

studies reveal a key difference in motion processing between the two species that must be taken into account in future mouse studies.

Compared to macaque, mice have a 100 fold lower SF tuning, with mouse V1 neurons preferring SFs around 0.03 cpd and macaque V1 neurons preferring SFs around 3 cpd (Niell and Stryker, 2008; Gao et al. 2010; Foster et al., 1985; Xing et al., 2004). This difference in SF tuning suggests that mouse V1 neurons are not capable of extracting the same quality of information about objects moving in their environment, particularly edges which have high SF harmonics. Differences in eye movements between these species may also explain differences in motion processing. Macaques have forward facing eyes and can make rapid saccadic eye movements to orient their fovea to a particular target (Fuchs, 1985; Schall et al., 1995), and are then capable of tracking objects via smooth pursuit (Komatsu and Wurtz, 1988; Schlack et al., 2008). On the other hand, mice have laterally positioned eyes lacking a fovea and their eye movements are limited to about 2° (van Alphen et al., 2001; Andermann et al., 2011). From the above, it might be tempting to conclude that differences in V1 speed tuning between macaque and mice are due to differences in the eye and brain of the two species, perhaps driven by their distinct ecology. However, not all primates show comparable amounts of speed tuning in V1 neurons to macaques. For example, less than 5% of neurons in marmoset V1 are speed tuned (Yu et al., 2010). Since marmosets are new world monkeys, there might then be a division in the level of speed processing in the early visual cortex between old world monkeys and other mammals. Speed tuning is also rare in area 17/18 of

the cat (Holub and Morton-Gibson 1981; Friend and Baker 1993), which further substantiates this division.

In the mouse, extrastriate region PM has many speed tuned neurons, and speed tuning in area PM has been correlated with the behavioural profile of speed perception in this species (Umino et al., 2008; Andermann et al., 2011). In primates, there is also an increase in speed processing in extrastriate motion areas: in macaques speed tuning is 1-2 times more common in MT than V1 (Priebe et al. 2003; Priebe et al. 2006), and in marmosets speed tuning is 2-6 times more common in MT than V1 (Lui et al., 2007; Yu et al., 2010). There is evidence in macaque that MT has a direct role in speed perception (Liu and Newsome 2005), so it may be the case that the increased representation of stimulus speed in extrastriate motion regions parallels the tighter link between these regions and speed perception across species.

In this study we measured spatiotemporal tuning in mouse primary visual cortex using single unit *in vivo* electrophysiology. Similar to a recent two-photon calcium imaging study by Andermann et al. (2011), we show that mice have very few speed selective neurons in V1 compared to macaque (Priebe et al., 2006). Although mice differ from macaques with regard to the proportion of inseparable V1 neurons, there is evidence that speed tuning is more common in specialized motion-coding extrastriate regions of both species (PM in mouse; MT in primates). Despite the differences in V1 speed processing between species, mice are still an attractive model of cortical motion processing because they represent a genetically tractable system in which the entirety of the motion processing stream can be

imaged (e.g. calcium imaging) or recorded (e.g. multi-electrode arrays) simultaneously. These technical options may facilitate progress in our understanding of the neural coding for stimulus speed, and how motion is processed at different stages of the visual pathway.

CHAPTER 3 DEPENDENCE OF CONTRAST ADAPTATION ON SPATIOTEMPORAL TUNING IN MOUSE V1

3.1 Introduction

Adaptation is a form of short-term visual plasticity whereby the visual system alters its sensitivity to certain stimulus features to allow for optimal processing of the visual scene based on recent viewing conditions. One visual feature that drives the response of V1 neurons is image contrast. Although adaptation to contrast is a ubiquitous phenomenon in the visual system, the underlying neural mechanisms of contrast adaptation are not well understood.

Contrast adaptation has been reported in the retina and dLGN, but is thought to be primarily a cortical phenomenon (Duong and Freeman, 2007; Kohn, 2007; Demb, 2008). After being adapted, V1 neurons exhibit about a seven times greater reduction in response compared to neurons of the dLGN (Dean, 1983; Nelson, 1991; Shou et al., 1996; Ahmed et al., 1997; Heinrich and Bach, 2001). Contrast response functions of V1 neurons can be described by plotting response amplitude as a function of stimulus contrast (Ohzawa et al., 1982), and it is well known that cat and macaque V1 neurons have sigmoidal contrast response functions (Bonds, 1991; Sclar et al., 1989). Adaptation is often measured by comparing the semi-saturation contrast, known as the c_{50}, for non-adapted and adapted responses, and contrast adaptation is characterized by a distinctive shift in this c_{50} value to center a neuron's contrast response function on the prevailing contrast.

As mentioned in the general introduction (Chapter 1, Section 1.3.3), the dependence of cortical contrast adaptation on the orientation, SF and TF of the

adaptor has been previously investigated (Movshon and Lennie, 1979; Albrecht et al., 1984; Marlin et al., 1988; Dragoi et al., 2000), although TF dependence has been the focus of fewer studies (Maddess et al., 1988; Saul and Cynader, 1989b). Traditionally, the dependence of contrast adaptation on SF and TF has been assessed using a preferred test stimulus, and a small number of adapting stimuli that straddled the neuron's peak SF or TF (Movshon and Lennie, 1979). Maximum adaptation has been reported to occur when the SF and TF of the adapting grating is similar to the SF and TF of the test grating (Movshon and Lennie, 1979; Saul and Cynader, 1989a,b), although thus far studies of the specificity of contrast adaptation have varied SF and TF independently. Stimuli distant from the preferred cause less firing when used as an adaptor, and generally induce less adaptation. The observation that the strength of adaptation depends on the similarity between the adapting and test stimulus is often thought of as a distinctive feature of adaptation. However, studies are now revealing that different adaptation effects may arise because specific cell populations adapt to stimuli in distinct ways.

A recent study by Dhruv et al. (2011) has suggested that different cell types show unique adaptation effects, resulting in varied changes in the shapes of their contrast response functions. Therefore, Dhruv et al. (2011) proposed that manipulating stimulus adaptors could reveal these distinct cell populations. It may be possible to test this hypothesis in mice if it were possible to manipulate these cell populations genetically to link specific cell types to contrast adaptation effects. While powerful genetic tools exist in the mouse, to use this model to investigate the circuit mechanisms underlying contrast adaptation, we must explore the

phenomenon as it occurs in mouse V1. Although mice are becoming a popular model for visual cortical processing, little research has investigated contrast adaptation in mouse V1. Orientation selectivity of contrast adaptation has been shown in mice (Stroud et al., 2012), but the influence of SF and TF has not yet been examined.

In order to investigate the spatiotemporal dependence of contrast adaptation, we first established the baseline spatiotemporal tuning of mouse V1 neurons, and then used a contrast ramp procedure to adapt and test neurons at 36 different spatiotemporal combinations. This contrast ramp procedure allows for the timely measurement of responses to dynamic contrast changes, which have been previously shown to elicit contrast adaptation in V1 neurons (mouse: Stroud et al., 2012, cats: Crowder et al., 2008). Typically, contrast adaptation is tested with prolonged exposure to a single contrast followed by brief tests, which take a long time for each adapting stimulus making it difficult to test multiple SFs and TFs. However, dynamic contrast ramp stimuli can measure contrast adaptation evoked by a single stimulus in a matter of seconds, and are therefore useful in testing how multiple SFs and TFs affect adaptation in a single neuron. Furthermore, it has been proposed that contrast ramps more closely mimic the type of gradual contrast changes invoked when viewing natural scenes (Crowder et al., 2008). Because we were interested in whether our population of neurons adapted maximally to the same spatiotemporal frequency to which they fired maximally, we calculated the octave difference between the location of the preferred spatiotemporal frequency and the spatiotemporal location of maximum hysteresis. We found that there was often a difference between the grating that elicited the greatest firing, and the

grating where adaptation was most pronounced, such that adaptation was usually stronger at higher SFs.

3.2 Materials And Methods

3.2.1 Animals

Electrophysiological recordings were made from 17 C57BL/6J mice. Data for this experiment was collected from the same neurons presented in experiment 1; therefore the same animals were used.

3.2.2 Surgical And Physiological Preparation

All details of surgery, life support, and electrophysiological techniques can be found in Chapter 2, Section 2.2.2.

3.2.3 Visual Stimuli

All stimuli used for testing were custom made using the psychophysics toolbox extension (Brainard, 1997; Pelli, 1997) of Matlab (MathWorks, Natick MA) and presented on a CRT monitor (LG Flatron 915FT plus, 100Hz refresh, 1024x768 pixels). All experimental stimuli were presented in a circular aperture, surrounded by a grey field of mean luminance (30 cd/m^2). The viewing distance for each unit varied, and depended on the location of the receptive field, but generally ranged from 15 – 35 cm. Extracellular signals from individual units were amplified and filtered, and sent to an oscilloscope and an analog-digital converter, as described in experiment 1 (Chapter 2, Section 2.2.3). The receptive fields of visually responsive units were mapped using a hand held light bar, and then the orientation selectivity and surround suppression of each unit was characterized online with drifting square wave gratings. Spatiotemporal tuning was also characterized online with

drifting sine wave gratings in order to determine the unit's preferred spatiotemporal frequency. We used 36 combinations of SFs (0.01, 0.02, 0.04, 0.16 and 0.32 cpd) and TFs (0.25, 0.5, 1, 2, 4 and 8 Hz). Spatiotemporal stimuli were presented at the optimal orientation and patch size for each unit and presentations of each combination were randomized with 8 – 10 repeats per combination.

3.2.3.1 Contrast Ramps

Michelson contrast is defined by the following equation:

$$\textit{Michelson Contrast} = \frac{\mathrm{Lum_{max}}\text{-}\mathrm{Lum_{min}}}{\mathrm{Lum_{max}}+\mathrm{Lum_{min}}} \quad (6)$$

where $\mathrm{Lum_{max}}$ is the maximum luminance and $\mathrm{Lum_{min}}$ is the minimum luminance. When contrast is 0, the screen appears as a homogeneous grey. When contrast is 1, the amplitude of the sine wave has reached its maximum and this describes the maximum difference in luminance values that can be presented on the monitor. In this study, we wished to characterize how contrast adaptation is affected by the spatiotemporal characteristics of the adapting and test stimulus. Traditional methods of inducing contrast adaptation rely on prolonged presentations of the adapting stimulus (Sclar et al., 1989, 1990; Sanchez-Vives 2000a), therefore exploring the dependence of contrast adaptation on both stimulus SF and TF simultaneously would require very long recording times. To rapidly assess the nature of contrast adaptation in the spatiotemporal domain, we used dynamic contrast ramp stimuli. Contrast ramps have recently been shown to rapidly measure several important markers of contrast adaptation with fairly short presentation times (Crowder et al., 2008; Stroud et al., 2012). In this study, contrast ramp stimuli consisted of sine wave gratings that were presented at the preferred orientation and

patch size for each unit, and grating drift occurred perpendicular to the unit's preferred direction. Unlike the contrast step stimuli used to obtain spatiotemporal response profiles, contrast ramp stimuli present a dynamic range of contrasts over the presentation time of the stimulus. Contrast ramp stimuli were first presented at a contrast of 0, and contrast was increased linearly over 2 seconds until it reached 1 (rising phase). The contrast of the stimulus was then ramped back down from 1 to 0 (falling phase) over the next 2 seconds (Figure 5). A full screen grey of mean luminance was shown between ramp stimuli for 1 second. Contrast ramps were carried out for each of the 36 spatiotemporal combinations, and presentations of contrast ramps with different spatiotemporal combinations were randomized and repeated 8 – 10 times for each combination.

We were interested in determining whether the spatiotemporal combination that caused maximal firing also caused maximum hysteresis. In order to test this, we used a *symmetrical* contrast ramp procedure, which maintained the same spatiotemporal parameters for both the rising and falling phase of the ramp. In addition, we were interested in whether the spatiotemporal frequency of the test stimulus affected contrast adaptation. In order to control for this, we collected *peak-tested* contrast ramps from a subset of neurons in which the rising phase of the ramp was one of the 36 combinations of varying spatiotemporal frequencies, but the test stimulus (falling phase) was always shown at the neuron's preferred SF and TF (See Results), as calculated from the online tuning function.

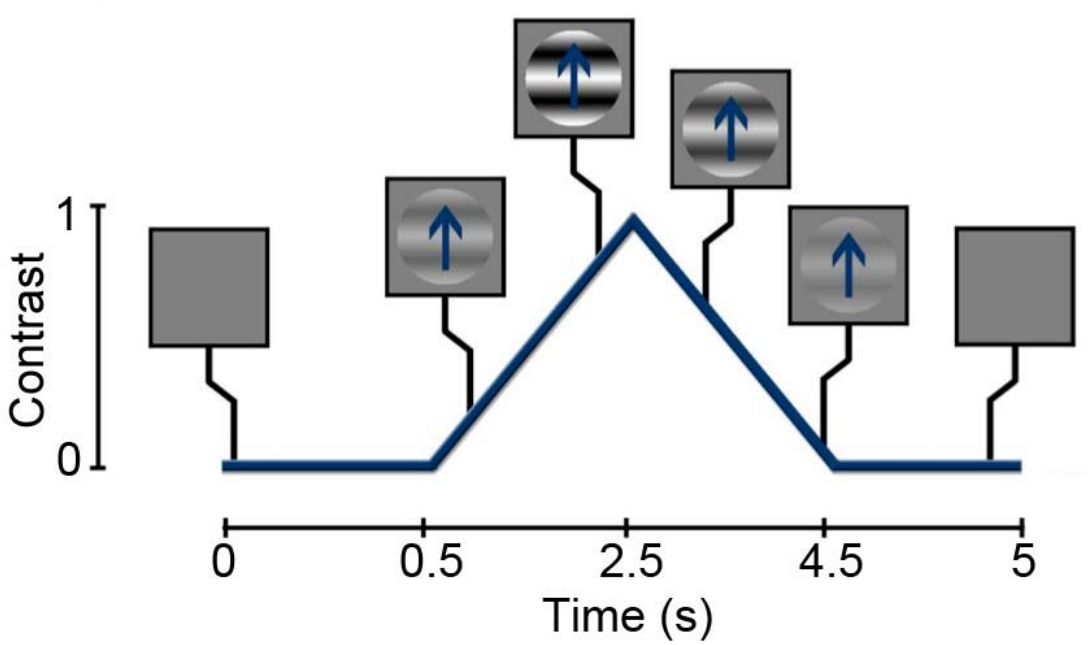

Figure 5. Schematic Diagram of Contrast Ramps. Stimulus contrast was linearly increased from 0 to 1 over two seconds and then ramped back down from 1 to 0 over the following two seconds. Total presentation time was 5 seconds, as 0.5 seconds of homogenous grey separated each ramp stimulus. Grating drift was always perpendicular to a unit's preferred orientation.

3.2.4 Initial Data Analysis

As in experiment 1, Spike2 (Cambridge Electronic Design) was used to complete spike sorting, and a principle components analysis was performed in order to isolate single units.

3.2.4.1 Strength Of Tuning For Orientation And Patch Size

For each unit, we calculated the degree of orientation and size tuning using a discrimination index (DI) (DeAngelis and Uka, 2003):

$$\text{Discrimination Index} = \frac{(Resp_{Max} - Resp_{Min})}{((Resp_{Max} + Resp_{Min}) + 2\sqrt{SSE}/(N-M))} \quad (7)$$

$Resp_{Max}$ and $Resp_{Min}$ are the neuron's maximum response and minimum response, respectively. SSE is the sum of squared error of the mean, N is the total number of presentations of the stimuli, and M is the number of different stimuli presented.

3.2.4.2 Spatial Summation

We classified cells as simple or complex by dividing the first Fourier coefficient of a neuron's response to a sine wave grating presented at the spatiotemporal peak (F_1) by the mean time-averaged response to the grating (F_0). The F_1/F_0 ratio has been used in previous studies to categorize cells as either simple or complex (Schiller et al., 1976; Skottun et al., 1991; Movshon et al., 1978a,b). Complex and simple cells have F_1/F_0 ratios less than 1 and greater than 1, respectively.

3.2.4.3 Neural Latency

In order to calculate neural latency, we first determined the spontaneous rate of each unit from the activity during a half second grey screen prior to drifting sine wave grating onset during the spatiotemporal tuning procedure. A Poisson

distribution was fitted to the spontaneous firing that occurred during the half second grey screen and this was used to calculate a response threshold. Neuronal latency was then calculated by determining when the firing rate exceeded and was maintained above this calculated threshold for at least 25 ms (Price et al., 2005). Contrast ramps were shifted back in time by a unit's calculated neural latency and split into the rising and falling phases. The falling phase was folded back onto the rising phase in order to compare non-adapted and adapted responses, and the x-axis then represented stimulus contrast.

3.2.4.4 Curve Fitting

A least squares method was used to fit SDFs for both the rising (pre-adaptation) and falling (post-adaptation) phase of the ramp (Albrecht and Hamilton, 1982), as described by the Naka-Rushton equation:

$$R(c_i) = \frac{R_{max} \times c_i^n}{c_i^n + c_{50}^n} + S \qquad (8)$$

where $R(c_i)$ is the amplitude of the response to the contrast c_i, R_{max} is the maximum rate of firing, c_{50} describes the contrast at half of the R_{max} value and n is the slope of the curve at the c_{50}. Finally, S is the spontaneous activity of the neuron. Curve fitting was carried out for contrast ramp responses to each of the 36 spatiotemporal combinations in order to examine adaptation at each unique combination. r^2 was used as a measure of goodness of fit for rising and falling fits at a unit's preferred spatiotemporal frequency.

3.3 Results

Spatiotemporal profiles reported in Chapter 2 were the control condition in this experiment, and were always collected first. Contrast ramp data was collected

second, and we obtained full data sets for 122 cells: 90 *symmetrical* ramps, and 32 *peak-tested* ramps. The discrepancy between the numbers of units for which complete data sets were recorded in experiment 1 (146) compared to experiment 2 (122) was caused by the premature loss of unit isolation during the recording of contrast ramp responses due to the additional time it took to record contrast ramps.

The subset of V1 neurons from which we collected ramps had similar orientation and size tuning compared to our general population measures (Chapter 2, Section 2.4). The median DI for cells in the ramp procedure was 0.49 and 0.57 for orientation and size tuning, respectively. Using a one-way ANOVA, we found that only 9 cells in the ramp procedure showed significant surround suppression ($F_{(1,14)} \geq 5.2$, $p < 0.05$). From cells which we collected ramps, only 4% were simple cells and the remainder were complex. There was no difference between responses of either cell type, so simple and complex cells were pooled for the remaining analyses. The mean onset latency calculated for our population of V1 neurons was 82.6 ± 56.8 ms, which is comparable to the onset latency reported by Gao et al. (2010).

3.3.1 Spatiotemporal Tuning

The spatiotemporal profile of each neuron allowed us to determine the combination of SF and TF that elicited maximum firing for each unit when contrast remained constant. As reported in experiment 1, peak SFs and TFs were broadly distributed, with preferred SFs that ranged from 0.01 to 0.17 cpd (mean = 0.03 cpd), and TFs that ranged from 0.25 to 8 Hz (mean = 1.77 Hz).

Figure 6A shows a spatiotemporal profile for a representative unit, with a SDF for each of the 36 combinations of spatiotemporal frequencies. The mean

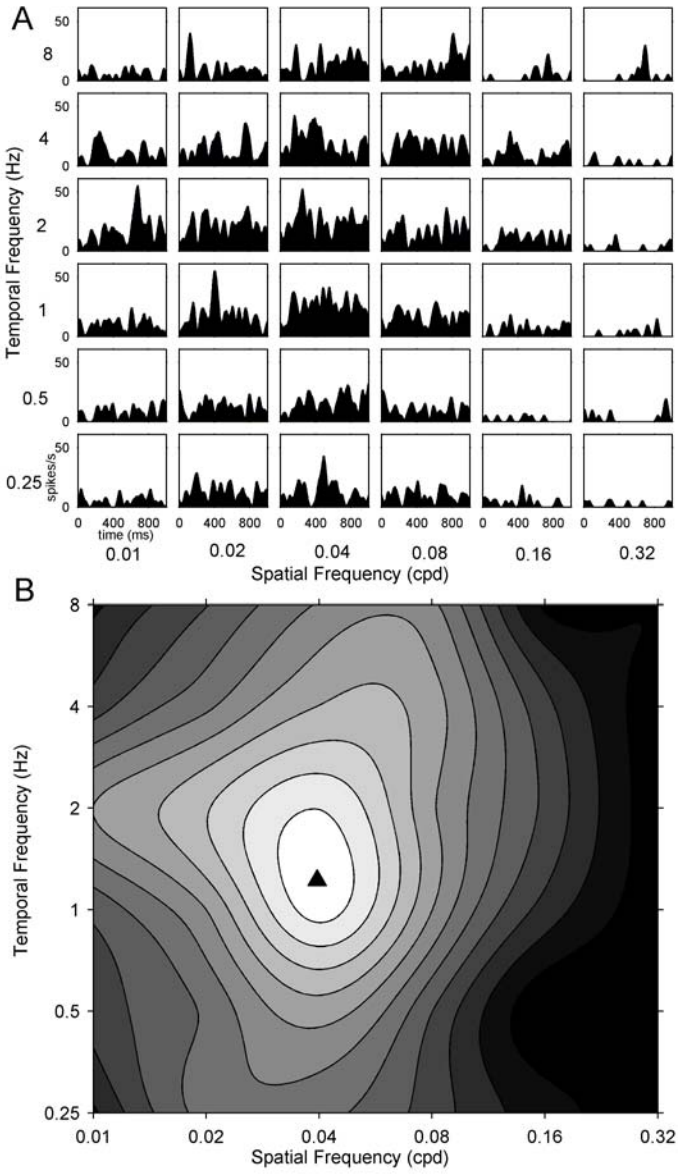

Figure 6. Spatiotemporal tuning of mouse V1 neurons. A shows the spatiotemporal profile for a representative neuron with spatial frequency on the abscissa and temporal frequency on the ordinate. The response to each of 36 spatiotemporal combinations is shown as a SDF. The mean data from A is summarized as a contour plot in B. The peak preferred spatiotemporal frequency is indicated by a closed triangle, and this neuron preferred SFs of around 0.04 cpd and TFs of around 1 Hz (B).

response to each of the 36 combinations was summarized as a contour plot (Figure 6B), and it is evident this neuron preferred SFs of around 0.04 cpd and TFs of around 1 Hz.

3.3.2 Response to Contrast Ramps

After we obtained the spatiotemporal profile of a neuron, we collected *symmetrical* contrast ramps at each of the 36 spatiotemporal frequencies in order to test for contrast adaptation at each unique combination. Figure 7A shows a typical symmetrical ramp response obtained near the preferred SF and TF of a sample neuron. A considerable degree of hysteresis is evident in this response, and this effect was further emphasized when the response to the falling phase was flipped left-to-right and re-plotted (Figure 7B). We fit both the rising and falling phases of ramps to a sigmoidal function, as indicated by the thin lines in Figure 7B. Sigmoidal fits became poorer as the SF and TF combination being presented deviated away from the spatiotemporal peak of each neuron due to lower responsivity at these non-preferred SF and TF combinations. Therefore, c_{50} values were only extracted from sigmoid fits to responses at the neuron's peak SF and TF. The c_{50} values for the rising and falling phases are represented in Figure 7B by the upward and downward facing triangles, respectively. The c_{50} values from the rising phase were significantly smaller than the c_{50} values from the falling phases for a neuron's peak spatiotemporal frequency (paired t test, $p < 0.001$, $df = 89$), and this is consistent with earlier observations of ramp responses in mice and cats (Stroud et al., 2012; Crowder et al., 2008).

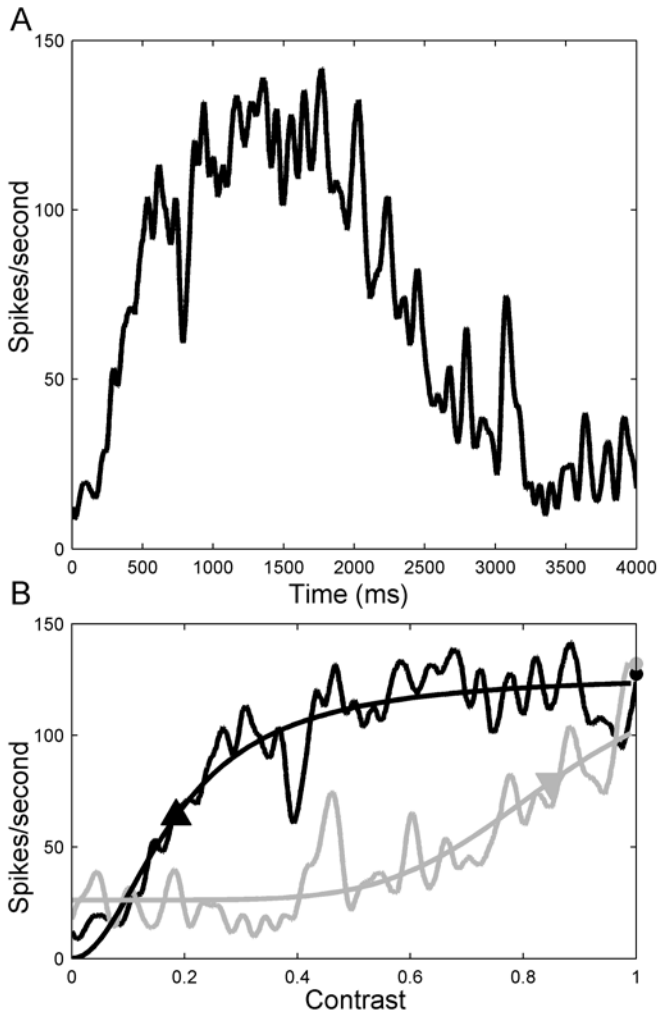

Figure 7. Response to contrast ramps. A shows the response for a representative neuron to the rising and falling portions of the contrast ramp as a SDF. During the rising portion contrast is linearly ramped up from 0 to 1 and during the falling portion back down from 1 to 0. In B, the data from A is shifted back in time by the unit's calculated neural latency and the falling portion of the ramp is flipped from left to right. Both the rising (black) and falling (grey) portions of the contrast ramp response are fit with sigmoidal functions, and the black upward and grey downward facing triangles represent c_{50} values obtained from fits to the rising and falling responses, respectively. The rightward shift in c_{50} is a hallmark of contrast

adaptation. The black and grey filled circles represent R_{max} values taken from the sigmoid fit to the rising and falling phases, respectively.

For the *symmetrical* ramps we were interested in whether maximum hysteresis occurred at the preferred spatiotemporal frequency of the neuron. Since measures of c_{50} were unreliable for spatiotemporal combinations away from the peak, we measured adaptation by calculating the mean difference between the rising and falling phases of the contrast ramps. During adaptation, the semi-saturation contrast of the falling phase ramp response shifts to higher values, causing the falling ramp response to be lower than the rising phase response at most contrasts. This method of analysis has been shown by Stroud et al. (2012) to capture the major features of contrast adaptation without relying on fitting the ramp SDFs to sigmoid functions. Figure 8A shows a grid of 36 ramp responses to all 36 combinations of SFs and TFs. Rising phases are shown as black lines, falling phases are shown as grey lines, and it is obvious that for nearly every combination falling phase responses are below rising phase responses. The mean difference between the response to the rising and falling portions of the ramp, for each of the 36 combinations, were summarized as a contour plot in figure 8B, and the location of maximum hysteresis is readily apparent (SFs of 0.04 cpd and TFs of 1 Hz).

For neurons from which we collected both spatiotemporal tuning and a ramp hysteresis profile, it was possible to compare the spatiotemporal locations of maximum firing and maximum hysteresis. For the sample neuron shown in figure 9AB, it appeared that adaptation was maximal at a spatiotemporal location different from the peak spatiotemporal frequency, but for the neuron shown in 9CD the spatiotemporal peak locations were similar. In order to quantify whether our population of neurons adapted maximally to the same spatiotemporal frequency to

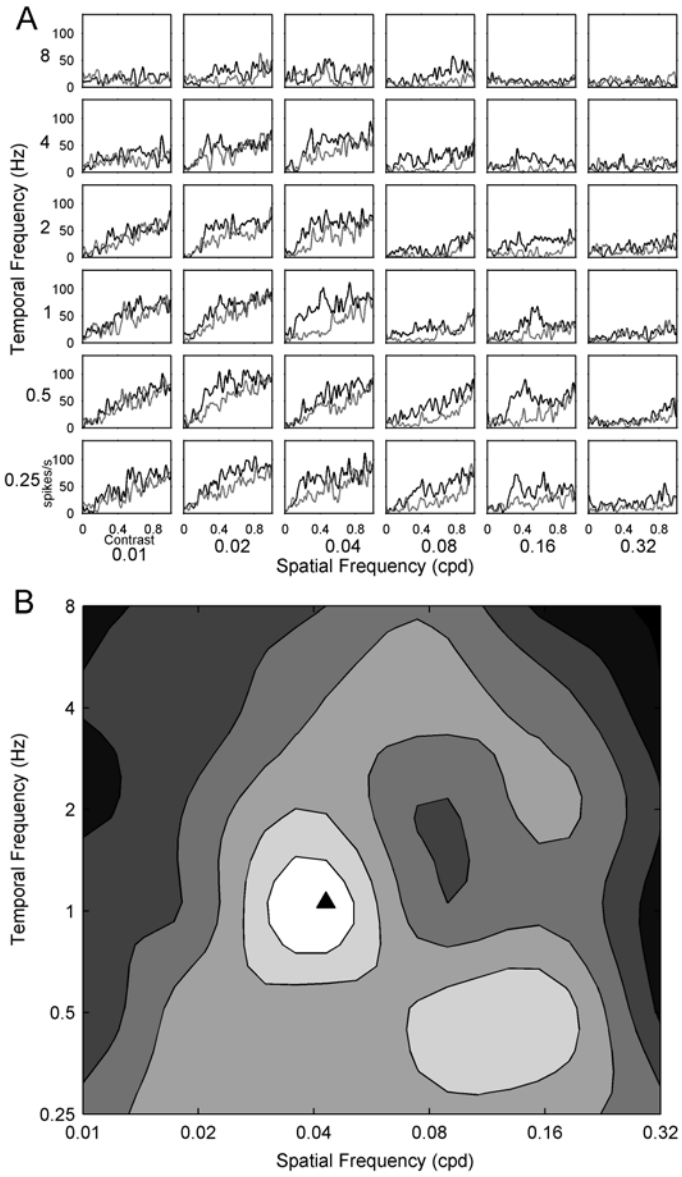

Figure 8. Hysteresis profile of mouse V1 neurons. A shows the hysteresis profile for an example neuron where the response to rising (black) and falling (grey) phases of contrast ramps at 36 spatiotemporal combinations is shown as a SDFs as in figure 7B. The largest difference between rising and falling responses occurs around SFs of 0.04 cpd and TFs of 1 Hz. The mean difference between rising and falling phases is summarized as a contour plot in B (See Results). The spatiotemporal location of maximum hysteresis is indicated by a closed triangle.

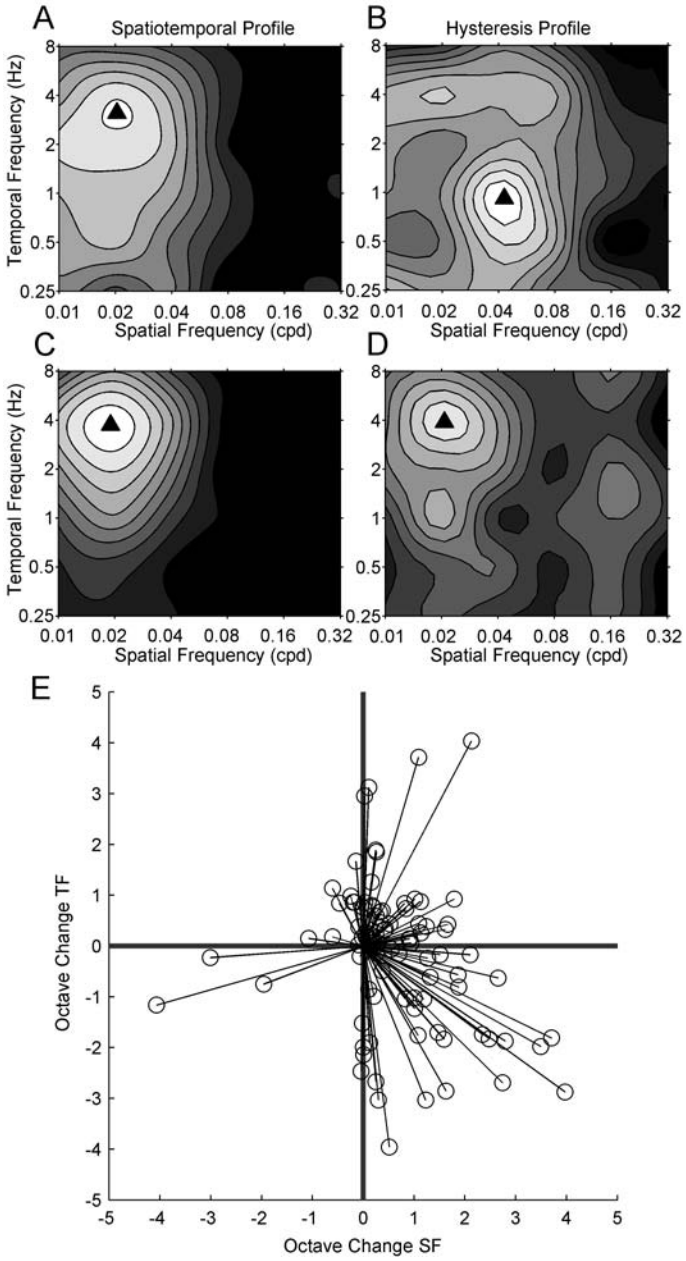

Figure 9. Comparison of peak spatiotemporal frequency and maximal hysteresis for *symmetrical* contrast ramps. A-D compare the spatiotemporal and hysteresis profiles for two representative neurons (rows). The peak spatiotemporal frequencies are represented by closed triangles. For the neuron shown in A and B, there is a readily apparent difference between the location of the optimal spatiotemporal frequency from the tuning procedure (SF: 0.02 cpd, TF: 3 Hz) and

the spatiotemporal location of maximum hysteresis from the contrast ramp procedure (SF: 0.04 cpd, TF: 1 Hz). For the neuron shown in C and D there is substantial overlap between the optimal spatiotemporal frequency (SF: 0.02 cpd, TF: 4 Hz) and the spatiotemporal location of maximum hysteresis for this neuron (SF: 0.02 cpd, TF: 4 Hz). In order to quantify this difference between the location of the peak spatiotemporal response and the spatiotemporal location of maximum hysteresis, we calculated the octave difference in SFs and TFs for our population of V1 neurons, as summarized in E. Across the population, maximal contrast adaptation usually occurred at higher SFs than the spatiotemporal peak.

which they fired maximally, we calculated the octave difference in peak SF and TF between the spatiotemporal tuning and contrast ramp contour plots. The spatiotemporal peak of each neuron was normalized to zero, and the peak from the hysteresis profile was plotted as a vector from this origin (Figure 9E). For the *symmetrical* ramps the average octave difference in peak spatiotemporal frequency between the tuning and ramp procedure was 0.65 and -0.19 octaves for SF and TF, respectively. Only the octave change in SF was significantly different from zero, and maximal adaptation appeared to consistently occur at higher spatial frequencies (paired t tests, $p < 0.001$, Bonferroni correction critical p value = 0.0125). While many of the cells that had large differences between the spatiotemporal profile and the hysteresis profile appeared to adapt more to lower temporal frequencies, this change in TF was not significantly different from zero (paired t test, $p = 0.67$, Bonferroni correction critical p value = 0.0125).

Earlier studies that have used top-up protocols to measure adaptation had a test stimulus that was of the preferred SF or TF of the cell. These studies showed that maximal adaptation occurred when the adapting stimulus was similar to the test stimulus (Movshon and Lennie, 1979; Albrecht et al., 1984; Maddess et al., 1988; Saul and Cynader, 1989a). Because these studies made use of test stimuli that was of the optimal SF or TF, maximal adaptation appeared to occur at this combination. Many neurons in our symmetrical ramp procedure showed maximal adaptation away from their spatiotemporal peak when the falling phase of each ramp was different, so we used an additional ramp condition to control for the effect of the falling phase (test stimulus) on the measure of adaptation. For these *peak-*

tested ramps the rising phase was one of the 36 combinations of spatiotemporal frequencies, but the falling phase (test stimulus) was always shown at the neuron's preferred spatiotemporal frequency (obtained in the spatiotemporal tuning procedure). This stimulus allowed for a more direct comparison to previous tests that used a test stimulus of the preferred SF or TF. For *peak-tested* ramps we also fit rising and falling contrast ramp responses at the peak SF and TF to sigmoidal functions, and adaptation was apparent just like in the *symmetrical* ramps, as the c_{50} values from the rising phase of *peak-tested* ramps were significantly smaller than the c_{50} values from the falling phases for a neuron's optimal spatiotemporal frequency (paired t test, $p < 0.001$).

Unlike with the *symmetrical* ramps, where the rising and falling phases were always maintained at the same spatiotemporal frequency, in the *peak-tested* ramps the rising and falling phase matched for only one of 36 cases. To characterize adaptation for the *peak-tested* ramps, we instead compared the falling phase at the preferred spatiotemporal frequency to the falling phase at every other combination (Figure 10A). Therefore, for the one ramp stimulus in which the spatiotemporal frequency of the rising and falling phase matched (the neuron's preferred spatiotemporal frequency calculated in the tuning procedure), the difference between the two falling phases would be 0. When comparing the falling phases of all other ramps to the preferred falling phase, the difference would be large if no contrast adaptation occurred, or small if contrast adaptation did occur. We again represented adaptation at each unique combination as a contour plot, and compared this adaptation profile to each neuron's spatiotemporal profile. We then calculated

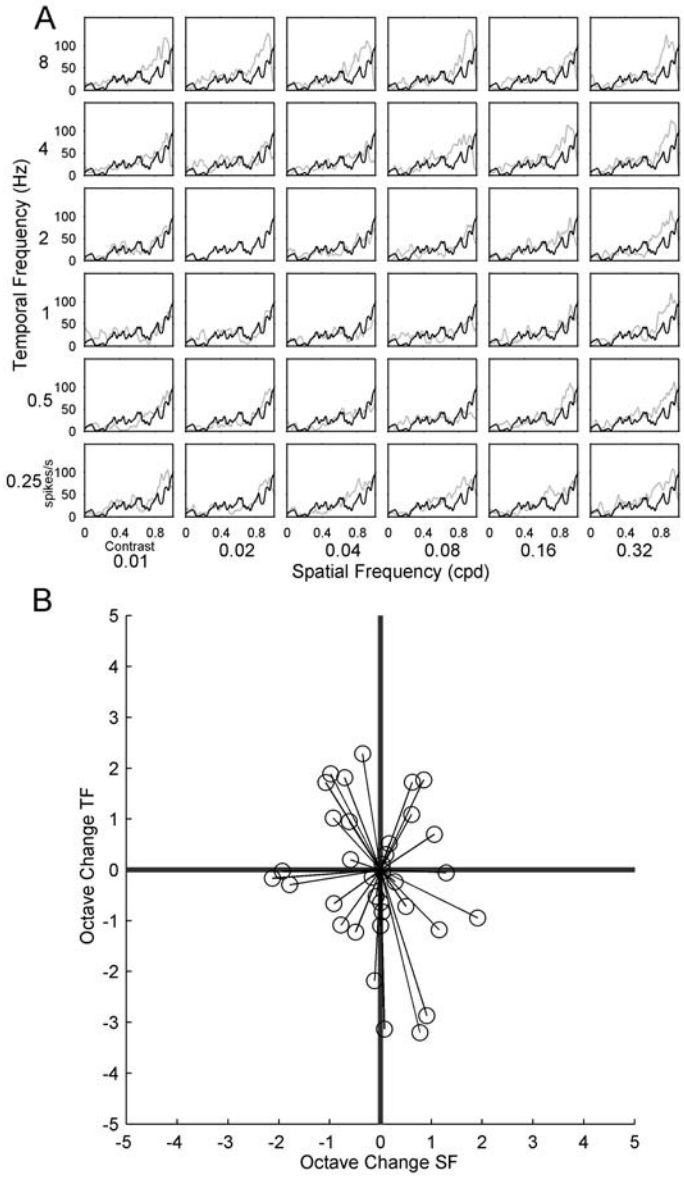

Figure 10. Comparison of peak spatiotemporal frequency and maximal adaptation for *peak-tested* contrast ramps. A shows the ramp responses for an example neuron in the *peak-tested* procedure. We compared the falling phase at the peak spatiotemporal frequency calculated in the tuning procedure (black) to the falling phases for the other 35 combinations of spatiotemporal frequencies (grey). Falling phase responses around the neuron's optimal spatiotemporal frequency (SF: 0.02 cpd, TF: 2 Hz) were similar in magnitude to the peak falling response, indicating that

the degree of adaptation was similar to that seen at the spatiotemporal peak. At spatiotemporal frequencies away from the peak, the response to the other falling phases is usually greater than the peak falling phase, indicating that less adaptation occurred. In order to calculate whether there was a difference in the optimal spatiotemporal frequency and the location of maximal hysteresis for V1 neurons in the *peak-tested* ramp condition, we calculated the octave change in SF and TF (B). There was no consistent change in SF or TF, and preferred spatiotemporal frequency was similar to the spatiotemporal location of maximal adaptation.

the octave difference in SF and TF for *peak-tested* ramps in order to determine whether there were any differences between the preferred spatiotemporal frequencies and the stimulus that produced maximal adaptation. For the *peak-tested* ramps, changes appeared smaller than those seen in the *symmetrical* ramp procedure, with a mean octave change of -0.09 and -0.15 for SF and TF, respectively (Figure 10B). For this control condition, the octave changes in SF and TF were not significantly different from zero (SF: $p = 0.66$, TF: $p = 0.43$; Bonferroni correction critical p value = 0.0125), which is similar to earlier studies that have shown adaptation is maximal at the preferred spatiotemporal frequency when the test stimulus is always shown at the optimal spatiotemporal frequency of a neuron.

3.4 Discussion

In this study we measured the dependence of contrast adaptation on spatial and temporal frequency simultaneously in mouse V1 neurons using single unit *in vivo* electrophysiology. We used a dynamic contrast ramp stimulus, which allowed for the collection of adaptation responses at each of 36 unique spatiotemporal combinations. This is novel in that previous studies have used top-up adaptation protocols that, due to their extended presentation time, allow for the collection of only a small set of spatial or temporal frequencies, which are tested independently of one another (e.g., Movhson and Lennie, 1979; Saul and Cynader, 1989a,b).

We were interested in determining whether the spatiotemporal frequency that elicited maximum firing to steady-state stimuli for a neuron also induced maximum contrast adaptation. Adaptation was evident as response hysteresis in the *symmetrical* ramp procedure, and in our population we found that adaptation was

usually strongest at a higher SF than the peak SF determined by spatiotemporal tuning. The results of our *symmetrical* contrast ramp were different from previous investigations that used a top-up protocol to measure adaptation and a test stimulus that was of the optimal SF or TF for the cell. These studies reported that maximum adaptation occurred when the adapting stimulus was similar to the test stimulus (Movshon and Lennie, 1979; Albrecht et al., 1984; Saul and Cynader, 1989a). The discrepancy between previous studies and our findings may be because these studies used test stimuli that were of the optimal SF or TF, which would result in maximal adaptation occurring at this combination. Therefore, we also used a *peak-tested* ramp in which the adapting stimulus was one of 36 combinations of spatiotemporal frequencies and the test stimulus (falling phase) was always shown at the neuron's optimal spatiotemporal frequency. When neurons were tested with this ramp procedure, we found no significant difference between the optimal spatiotemporal frequency collected in the tuning procedure and the spatiotemporal frequency that elicited maximum hysteresis, which is similar to what was shown in previous studies (Movshon and Lennie, 1979; Albrecht et al., 1984; Maddess et al., 1988).

Contrast adaptation can arise through both lateral shifts of a neuron's response function and decreases in maximal firing, which are called contrast gain control and response gain control, respectively (Bonds, 1991; Carandini and Ferster, 1997). There has been a range of mechanisms reported to underlie contrast adaptation, though conclusive evidence for any single mechanism is lacking. One proposed mechanism underlying response gain control is deleterious fatigue

(Carandini, 2000), where upon being exposed to a stimulus that causes maximal firing, a neuron becomes too metabolically taxed to continue firing at high levels (Albrecht et al., 1984; Carandini, 2000; Kohn, 2007). Perceptually, post-adapted stimuli are seen as weaker than the true contrast, which has been attributed to this reduction in neural responsivity. Changes in the response of a neuron can also be caused by lateral shifts in its contrast response function. This contrast gain control results in altered perception via shifts in the response function of a neuron, and not by a simple reduction in firing (Crowder et al., 2006). Unlike deleterious fatigue where the firing of a neuron is reduced and the contrast response function is shifted downward, the neuron can still achieve maximal firing even though it is in an adapted state. A proposed mechanism that could account for both response gain control and contrast gain control is a tonic hyperpolarization of the membrane potential, which is associated with negligible change in synaptic input (Carandini and Ferster, 1997; Sanches-Vives et al., 2000a,b). Electrophysiological studies in V1 have substantiated both reductions in dynamic range of a cell and reductions in contrast sensitivity, but support for the latter appears to be more widespread (cat: Dean, 1983; Crowder et al., 2006; macaque: Sclar et al., 1989). Similar to these previous studies, our results support a lateral shift in a neuron's response function, which could act to center a neuron's most sensitive range around the contrast of the adaptor (Sclar et al., 1989; Bonds, 1991; Crowder et al., 2006). We saw a significant lateral shift in c_{50} values in the falling phase compared to the rising phase of our ramp procedures. For the falling phase responses, c_{50} values were always shifted towards higher contrasts. In the *symmetrical* contrast ramps, the spatiotemporal

location of maximum adaptation was often separated from the spatiotemporal location of maximum firing. Under the assumptions of deleterious fatigue as a source of contrast adaptation, the stimulus that caused maximum firing would also be assumed to create maximum fatigue, and therefore adaptation. Because of the differences in spatiotemporal locations between maximum firing and adaptation in our data set our results do support deleterious fatigue, and may be better explained by contrast gain control. Contrast gain control would presumably readjust a neuron's sensitivity to contrast in order to center the dynamic range around the average contrast of recently viewed stimuli (Kohn, 2007).

The characteristics of contrast adaptation have been studied at the cortical level in various animal models, and have been described extensively in macaque V1 neurons (Sclar et al., 1989; Carandini et al., 1997; Sceniak et al., 1999) and cat V1 neurons (Maffei et al., 1973; Movshon and Lennie, 1979; Ohzawa et al., 1982; Carandini and Ferster, 1997; Crowder et al., 2006), but only recently in mice (Niell and Stryker, 2008; Stroud et al., 2012). Like in V1 neurons of other species, our results appear to support a spatiotemporal filter for contrast adaptation in mouse V1 neurons (Saul and Cynader, 1989b; Dhruv et al., 2011). The spatial filter we see in mice could represent the different adaptable cell populations described by Dhruv et al. (2011), and these cell populations appear to have different characteristics in different species. In macaque and cat V1, neurons have been reported to show stronger adaptation at high TFs (macaque: Dhruv et al., 2011; cat: Maddess et al., 1988). We instead found that mouse V1 neurons appear to adapt more at high SFs. Although there appears to be a species difference between adaptation

characteristics of V1 cell populations in mice and macaques, the idea of separate adaptable cell populations could still be tested in mice as long as these differences are taken into account.

Assuming that contrast adaptation is beneficial to visual perception, there must be a functional advantage provided by this phenomenon. One of several proposed functional benefits of contrast adaptation is that lateral shifts in the contrast response function would allow for neuron's to maintain maximum discriminability by shifting the most sensitive part of the response function to correspond to the prevailing contrast (the adaptor; Kohn, 2007). Lateral shifts in c_{50} have been consistently substantiated physiologically in V1 neurons of various species (cat: Crowder et al., 2006; macaque: Sclar et al., 1989; mouse: Stroud et al., 2012). However, perceptual data from psychophysical studies that support enhanced performance after adaptation is lacking, with inconsistent results demonstrating only weak or no enhancement in performance (contrast: Barlow et al., 1976; Määttänen and Koenderink, 1990; Abbonizio et al., 2001; orientation: Regan and Beverley, 1995; Clifford et al., 2001; Dragoi et al., 2002; motion: Clifford and Wenderoth, 1999; Hol and True, 2001). The finding that contrast adaptation appears to be stronger at higher SFs (than those that produce maximal firing) could act to preserve visual acuity in the mouse, and for this species improved contrast discrimination may depend on the spatial frequency of the adaptor. This perceptual benefit may be more readily testable in mice, compared to larger mammals, because of access to a combination of genetic, physiological, and psychophysical techniques in this species.

CHAPTER 4 CONCLUSIONS

Traditionally, cortical visual processing has been studied in non-human primates and cats. The purpose of the research presented in this thesis was to characterize spatiotemporal tuning and contrast adaptation in mouse V1 neurons. Though mice have been historically neglected in vision research, the mouse model is now becoming an attractive alternative to cats and primates due to the ability to create conditional knock outs/ins, and genetically target specific cell types and circuits. To make use of the mouse as a model of visual processing, we must examine the basic visual properties of mice so that we can measure deviations from normal functioning induced by genetic manipulation, and make comparisons to higher mammals.

Probing the interaction between spatial and temporal frequency tuning in V1 neurons provides a strategy to characterize how aspects of the visual scene, such as motion, are processed. We are able to test these interactions by examining the selectivity of neurons to sine-wave gratings of different spatial and temporal frequencies. A recent study using calcium imaging in mouse V1 has revealed that neurons are not selective for stimulus speed (Andermann et al., 2011). Because this finding is in opposition to what has been described in macaque V1, we were interested in whether this result could be confirmed using standard electrophysiological techniques such as those used to measure speed tuning in macaque V1 (Priebe et al., 2006). In experiment 1, we used 36 different spatiotemporal frequencies to obtain representative spatiotemporal profiles for

mouse V1 neurons. Our results substantiate that any subset of neurons in mouse V1 selective for stimulus speed must be small. Consequently, our results do not support a transformation carried out at the level of V1 neurons in mice that is later inherited by extrastriate areas, such has been proposed in macaque (Priebe et al., 2006). In mouse V1, the lack of inseparable spatiotemporal tuning observed in this study, and also by Andermann et al. (2011), may support transformations carried out at the level of PM, or multiple extrastriate areas, as there is still a discrepancy between the spatiotemporal inseparability reported for area PM (Q = -0.36) and optomotor head-tracking sensitivity to speed (Q = -0.12; Umino et al., 2008). Therefore, our results support a qualitative difference between spatiotemporal transformations and inseparability in striate areas of mice and macaque.

In experiment 2, we characterized the dependence of contrast adaptation on spatiotemporal tuning in mouse V1. Single units were tested with a dynamic contrast ramp, which allowed us to measure the dependence of adaptation on both spatial and temporal frequency simultaneously. We showed that for most mouse V1 neurons there was a difference between the sine wave grating that elicited maximum firing, and the sine wave grating that caused maximum adaptation, such that adaptation was usually stronger at higher SFs. When adaptation was measured in neurons using a test stimulus of the optimal spatiotemporal frequency, we saw little difference between the grating that elicited maximal firing and the grating that caused maximum adaptation. Our measure of contrast adaptation at each of 36 unique spatiotemporal combinations represents the most complete parameterization of contrast adaptation in any species.

REFERENCES

Abbonizio G, Langley K, Clifford CW (2002) Contrast adaptation may enhance contrast discrimination. Spatial Vision 16: 45 – 58.

Ahmed B, Allison JD, Douglas RJ, Martin KAC (1997) An intracellular study of the contrast-dependence of neuronal activity in cat visual cortex. Cerebral Cortex 7: 559 – 570.

Albrecht DG, Farrar SB, Hamilton DB (1984) Spatial contrast adaptation characteristics of neurones recorded in the cat's visual cortex. Journal of Physiology 347: 713 – 739.

Albright TD, Stoner GR (1995) Visual motion perception. Proceedings of the National Academy of Sciences USA 92: 2433 – 2440.

Andermann ML, Kerlin AM, Roumis DK, Glickfield LL, Reid RC (2011) Functional specialization of mouse higher visual cortical areas. Neuron 72: 1025 – 1039.

Andersen RA (1997) Multimodal integration for the representation of space in the posterior parietal cortex. Philosophical Transactions of the Royal Society of London B Biological Sciences 352: 1421 – 1428.

Antonini A, Fagiolini M, Stryker MP (1999) Anatomical correlates of functional plasticity in mouse visual cortex. Journal of Neuroscience 19: 4388 – 4406.

Bair W, Movshon JA (2004) Adaptive temporal integration of motion in direction-selective neurons in macaque visual cortex. Journal of Neuroscience 24: 9305 – 9323.

Bair W, O'Keefe LP (1998) The influence of fixational eye movements on the response of neurons in area MT of the macaque. Visual Neuroscience 15: 779 – 786.

Balkema GW, Mangini NJ, Pinto LH, Vanable Jr. JW (1984) Visually evoked eye movements in mouse mutants and inbred strains. A screening report. Investigative Ophthalmology and Visual Science 25: 795 – 800.

Barlow HB, Macleod DI, van Meeteren A (1976) Adaptation to gratings: no compensatory advantages found. Vision Research 16: 1043 – 1045.

Beauchamp MS, Cox RW, DeYoe EA (1997) Graded effects of spatial and featural attention on human area MT and associated motion processing areas. Journal of Neurophysiology 78: 516 – 520.

Blakemore C, Campbell FW (1969) Adaptation to spatial stimuli. Journal of Physiology 200: 11 – 13.

Blakemore C, Muncey JP, Ridley RM (1973) Stimulus specificity in the human visual system. Vision Research 13: 1915 – 1973.

Blasdel G, Campbell D (2001) Functional retinotopy of monkey visual cortex. Journal of Neuroscience 21: 8286 – 8301.

Bonds AB (1991) Temporal dynamics of contrast gain in single cells of the cat striate cortex. Visual Neuroscience 6: 239 – 255.

Born RT, Bradley DC (2005) Structure and function of visual area MT. Annual Reviews of Neuroscience 28: 157 – 189.

Brainard DH (1997) The psychophysics toolbox. Spatial Vision 10: 433 – 436.

Britten KH, Shadlen MN, Newsome WT, Movshon JA (1992) The analysis of visual motion: a comparison of neuronal and psychophysical performance. Journal of Neuroscience 12: 4745 – 4765.

Britten KH, van Wezel RJA (2002) Area MST and heading perception in macaque monkeys. Cerebral Cortex 12: 692 – 701.

Busse L, Ayaz A, Dhruv NT, Katzner S, Saleem AB, Schölvinck ML, Zaharia AD, Carandini M (2011) The detection of visual contrast in the behaving mouse. Journal of Neuroscience 31: 11351 – 11361.

Bussey TJ, Saksida LM, Rothblat LA (2001) Discrimination of computer-graphic stimuli by mice: a method for the behavioural characterisation of transgenic and gene-knockout models. Behavioral Neuroscience 115: 957 – 960.

Calkins DJ, Sterling P (1999) Evidence that circuits for spatial and color vision segregate at the first retinal synapse. Neuron 24: 313 – 321.

Callaway EM (1998) Local circuits in primary visual cortex of the macaque monkey. Annual Reviews of Neuroscience 21: 47 – 74.

Carandini M, Ferster D (1997) A tonic hyperpolarization underlying contrast adaptation in cat visual cortex. Science 276: 949 – 952.

Carandini M, Heeger DJ, Movshon JA (1997) Linearity and normalization in simple cells of macaque primary visual cortex. Journal of Neuroscience 17: 8621 – 8644.

Carandini M, Heeger DJ, Movshon JA (1999) Linearity and gain control in V1 simple cells. In PS Ulinski, EG Jones and A Peters (Eds.), Cerebral Cortex, Volume 13: Models of cortical circuits, New York: Plenum.

Carandini M (2000) Visual cortex: fatigue and adaptation. Current Biology 10: 605 – 607.

Clifford CW, Wenderoth P (1999) Adaptation to temporal modulation can enhance differential speed sensitivity. Vision Research 39: 4324 – 4332.

Clifford CW, Wyatt AM, Arnold DH, Smith ST, Wenderoth P (2001) Orthogonal adaptation improves orientation discrimination. Vision Research 41: 151 – 159.

Conway BR, Chatterjee S, Field GD, Horwitz GD, Johnson EN, Koida K, Mancuso K (2010) Advances in color science: from retina to behavior. Journal of Neuroscience 30: 14955 – 14963.

Corbetta M, Miezin FM, Dobmeyer S, Shulman GL, Peterson SE (1990) Attentional modulation of neural processing of shape, color, and velocity in humans. Science 248: 1556 – 1559.

Corbetta M, Miezin FM, Dobmeyer S, Shulman GL, and Peterson SE (1991) Selective and divided attention during visual discriminations of shape, color, and speed: functional anatomy by positron emission tomography. Journal of Neuroscience 11: 2383 – 2402.

Crowcroft P (1966) Mice all over. London: Foulis.

Crowder NA, Price NSC, Hietanen MA, Dreher B, Clifford CWG, Ibbotson MR (2005) Relationship between contrast adaptation and orientation tuning in V1 and V2 of cat visual cortex. Journal of Neurophysiology 95: 271 – 283.

Crowder NA, Price NSC, Hietanen MA, Dreher B, Clifford CWG, Ibbotson MR (2006) Relationship between contrast adaptation and orientation tuning in V1 and V2 of cat visual cortex. Journal of Neurophysiology 95: 271 – 283.

Crowder NA, Hietanen MA, Price NSC, Clifford CWG, Ibbotson MR (2008) Dynamic contrast change produces rapid gain control in visual cortex. Journal of Physiology 586: 4107 – 4119.

Dean AF (1983) Adaptation-induced alterations of the relation between response amplitude and contrast in cat striate cortical neurons. Vision Research 23: 249 – 256.

DeAngelis GC, Ohzawa I, Freeman RD (1993) Spatiotemporal organization of simple cell receptive fields in the cat's striate cortex. II. Linearity of temporal and spatial summation. Journal of Neurophysiology 69: 1118 –1135.

DeAngelis GC, Uka T. (2003) Coding of horizontal disparity and velocity by MT neurons in the alert macaque. Journal of Neurophysiology 89: 1094 – 1111.

Demb JB (2008) Functional circuitry of visual adaptation in the retina. Journal of Physiology 586: 4377 – 4384.

De Valois RL, Albrecht DG, Thorell LG (1982) Spatial frequency selectivity of cells in macaque visual cortex. Vision Research 22: 545 – 559.

Dhruv NT, Tailby C, Sokol SH, Lennie P (2011) Multiple adaptable mechanisms early in the primate visual pathway. Journal of Neuroscience 31: 15016 – 15025.

Dräger UC (1975) Receptive fields of single cells and topography in mouse visual cortex. Journal of Comparative Neurology 160: 269 – 290.

Dräger UC, Olsen JF (1980) Origins of crossed and uncrossed retinal projections in pigmented and albino mice. Journal of Comparative Neurology 191: 383 – 412.

Dragoi V, Sharma J, Sur M (2000) Adaptation-induced plasticity of orientation tuning in adult visual cortex. Neuron 28: 287 – 298.

Dragoi V, Sharma J, Miller EK, Sur M (2002) Dynamics of neuronal sensitivity in visual cortex and local feature discrimination. Nature Neuroscience 5: 883 – 891.

Duong T, Freeman RD (2007) Spatial frequency-specific contrast adaptation originates in the primary visual cortex. Journal of Neurophysiology 98: 187 – 195.

Enroth-Cugell C, Robson JG (1984) Functional characteristics and diversity of cat retinal ganglion cells. Investigative Ophthalmology and Visual Science 25: 250 – 267.

Ferster D (1988) Spatially opponent excitation and inhibition in simple cells of the cat visual cortex. Journal of Neuroscience 8: 1172 – 1180.

Foster KH, Gaska JP, Nagler M, Pollen DA (1985) Spatial and temporal frequency selectivity of neurones in visual cortical areas V1 and V2 of the macaque monkey. Journal of Physiology 365: 331 – 363.

Fuchs AF (1967) Saccadic and smooth pursuit movements in the monkey. Journal of Physiology 191: 609 – 631.

Gao E, DeAngelis GC, Burkhalter A (2010) Parallel input channels to mouse primary visual cortex. Journal of Neuroscience 30: 5912 – 5926.

Gias C, Hewson-Stoate N, Jones M, Johnston D, Mayhew JE, Coffrey PJ (2005) Retinotopy within rat primary visual cortex using optical imaging. NeuroImage 24: 200 – 206.

Giese MA, Poggio T (2003) Neural mechanisms for the recognition of biological movements. Nature Reviews Neuroscience 4: 179 – 192.

Goodale MA, Milner AD (1992) Separate visual pathways for perception and action. Trends in Neuroscience 15: 20 – 25.

Gordon JA, Stryker MP (1996) Experience-dependent plasticity of binocular responses in the primary visual cortex of the mouse. Journal of Neuroscience 16: 3274 – 3286.

Haverkamp S, Wässle H, Duebel J, Kuner T, Augustine GJ, Feng G, Euler T (2005) The primordial, blue-cone color system of the mouse retina. Journal of Neuroscience 25: 5438 – 5445.

Hawken MJ, Shapley RM, Grosof DH (1996) Temporal-frequency selectivity in monkey visual cortex. Visual Neuroscience 13: 477 – 492.

Heinrich TS, Bach M (2001) Contrast adaptation in human retina and cortex. Investigative Ophthalmology and Visual Science 42: 2721 – 2727.

Hol K, Treue S (2001) Different populations of neurons contribute to the detection and discrimination of visual motion. Vision Research 41: 685 – 689.

Hubel DH, Wiesel TN (1962) Receptive fields, binocular interaction and functional architecture in the cat's visual cortex. Journal of Physiology 160: 106 – 154.

Hubel DH, Wiesel TN (1963) Shape and arrangement of columns in cat's striate cortex. Journal of Physiology 165: 559 – 568.

Hubel DH, Wiesel TN (1968) Receptive fields and functional architecture of monkey striate cortex. Journal of Physiology 195: 215 – 243.

Hubel DH, Wiesel TN (1974) Uniformity of monkey striate cortex: A parallel relationship between field size, scatter and magnification factor. Journal of Comparative Neurology 158: 295 – 306.

Hubel DH, Wiesel TN, Stryker MP (1978) Anatomical demonstration of orientation columns in macaque monkey. Journal of Comparative Neurology 177: 361 – 380.

Huberman AD, Niell DM (2011) What can mice tell us about how vision works? Trends in Neuroscience 34: 464 – 473.

Jeon CJ, Strettoi E, Masland RH (1998) The major cell populations of the mouse retina. Journal of Neuroscience 18: 8936 – 8946.

Kalatsky VA, Stryker MP (2003). New paradigm for optical imaging: temporally encoded maps of intrinsic signal. Neuron 38: 529 – 545.

Keeler CE (1924) The inheritance of a retinal abnormality in white mice. Proceedings of the National Academy of Sciences USA 10: 329 – 333.

Kiper DC, Fenstemaker SB, Gegenfurtner KR (1997) Chromatic properties of neurons in macaque area V2. Visual Neuroscience 14: 1061 – 1072.

Kohn A (2007) Visual adaptation: physiology, mechanisms, and functional benefits. Journal of Neurophysiology 97: 3155 – 3164.

Lisberger SG, Morris EJ, Tychsen L (1987) Visual motion processing and sensory-motor integration for smooth pursuit. Annual Review of Neuroscience 10: 97 – 129.

Liu J, Newsome WT (2005) Correlation between speed perception and neural activity in the middle temporal visual area. Journal of Neuroscience 25: 711 – 722.

Lui LL, Bourne JA, Rosa MGP (2007) Spatial and temporal frequency selectivity of neurons in the middle temporal visual area of new world monkey (Callithrix jacchus). European Journal of Neuroscience 25: 1780 – 1792.

Luo L, Callaway EM, Svoboda K (2008) Genetic dissection of neural circuits. Neuron 57: 634 – 660.

Maddess T, McCourt ME, Blakeslee B, Cunningham RB (1988) Factors governing the adaptation of cells in area 17 of the cat visual cortex. Biological Cybernetics 59: 229 – 236.

Maffei L, Fiorentini A, Bisti S (1973) Neural correlates of perceptual adaptation to gratings. Science 182: 1036 – 1039.

Mangini NJ, Pearlman AL (1980) Laminar distribution of receptive field properties in the primary visual cortex of the mouse. Journal of Comparative Neurology 193: 203 – 222.

Marlin SG, Hasan SJ, Cynader MS (1988) Direction-selective adaptation in simple and complex cells in cat striate cortex. Journal of Neurophysiology 59: 1314 – 1330.

Marshel JH, Garrett ME, Nauhaus I, Callaway EM (2011) Functional specialization of seven mouse visual cortical areas. Neuron 72: 1040 – 1054.

Martinez LM, Wang Q, Reid RC, Pillai C, Alonso JM, Sommer FT, Hirsch JA (2005) Receptive field structure varies with layer in the primary visual cortex. Nature Neuroscience 8: 372 – 379.

Määttänen LM, Koenderink JJ (1991) Contrast adaptation and contrast gain-control. Experimental Brain Research 87: 205 – 212.

Maunsell JHR, Van Essen DC (1987) The topographic organization of the middle temporal visual area in the macaque monkey: Representational biases and relationship to callosal connections and myeloarchitectonic boundaries. Journal of Comparative Neurology 266: 535 – 555.

McKee SP, Silverman GH, Nakayama K (1986) Precise velocity discrimination despite random variations in temporal frequency and contrast. Vision Research 26: 609 – 619.

Merigan WH, Katz LM (1990) Spatial resolution across the macaque retina. Vision Research 30: 985 – 991.

Métin C, Godement P, Imbert M (1988) The primary visual cortex in the mouse: receptive field properties and functional organization. Experimental Brain Research 69: 594 – 612.

Moldestad O, Karlsen P, Molden S, Storm JF (2009) Tracheotomy improves experiment success rate in mice during urethane anesthesia and stereotaxic surgery. Journal of Neuroscience Methods 176: 57 – 62.

Movshon JA, Thompson ID, Tolhurst DJ (1978a) Spatial summation in the receptive fields of simple cells in the cat's striate cortex. Journal of Physiology 283: 57 – 77.

Movshon JA, Thompson ID, Tolhurst DJ (1978b) Receptive field organization of complex cells in the cat's striate cortex. Journal of Physiology 283: 79 – 99.

Movshon JA, Lennie P (1979) Pattern-selective adaptation in visual cortical neurones. Nature 278: 850 – 852.

Nathans J (1999) The evolution and physiology of human color vision: insights from molecular genetic studies of visual pigments. Neuron 24: 299 – 312.

Nelson SB (1991) Temporal interactions in the cat visual system. II. Suppressive and facilitatory effects in the lateral geniculate nucleus. Journal of Neuroscience 11: 357 – 368.

Niell CM, Stryker MP (2008) Highly selective receptive fields in mouse visual cortex. Journal of Neuroscience 28: 7520 – 7536.

Ohzawa I, Sclar G, Freeman RD (1982) Contrast gain control in the cat visual cortex. Nature 298: 266 – 268.

Packer O, Hendrickson AE, Curcio CA (1989) Photoreceptor topography of the retina in the adult pigtail macaque (Macacu nemestrina). Journal of Comparative Neurology 288: 165 – 183.

Paxinos G, Franklin KBJ. The mouse brain in stereotaxic coordinates, New York: Academic, 2001.

Pelli DG (1997) The video toolbox software for visual psychophysics: transforming numbers into movies. Spatial Vision 10: 437 – 442.

Perrone JA, Thiele A (2001) Speed skills: measuring the visual speed analyzing properties of primate MT neurons. Nature Neuroscience 4: 526 – 532.

Perry VH, Cowey A (1984) Retinal ganglion cells that project to the superior colliculus and pretectum in the macaque monkey. Neuroscience 12: 1125 – 1137.

Porciatti V, Pizzorusso T, Maffei L (1999) The visual physiology of the wild type mouse determined with pattern VEPs. Vision Research 39: 3071 – 3081.

Price NS, Ono S, Mustari MJ, Ibbotson MR (2005) Comparing acceleration and speed tuning in macaque MT: physiology and modeling. Journal of Neurophysiology 94: 3451 – 3464.

Priebe NJ, Cassanello CR, Lisberger SG (2003) The neural representation of speed in macaque area MT/V5. Journal of Neuroscience 23: 5650 – 5661.

Priebe NJ, Lisberger SG, Movshon JA (2006) Tuning for spatiotemporal frequency and speed in directionally selective neurons of macaque striate cortex. Journal of Neuroscience 26: 2941 – 2950.

Prusky GT, West PWR, Douglas RM (2000) Behavioral assessment of visual acuity in mice and rats. Vision Research 40: 2201 – 2209.

Prusky GT, Douglas RM (2004) Characterization of mouse cortical spatial vision. Vision Research 44: 3411 – 3418.

Regan D, Beverley KI (1985) Postadaptation orientation discrimination. Journal of the Optical Society of America A 2: 147 – 155.

Reid RC, Alonso JM (1995) Specificity of monosynaptic connections from thalamus to visual cortex. Nature 378: 281 – 284.

Rodieck RW. The first steps in seeing, Sinauer Associates, 1998.

Rodieck RW, Watanabe M (1993) Survey of the morphology of macaque retinal ganglion cells that project to the pretectum, superior colliculus, and parvicellular laminae of the lateral geniculate nucleus. Journal of Comparative Neurology 338: 289 – 303.

Rowe MH (2002) Trichromatic color vision in primates. News in Physiological Sciences 17: 93 – 98.

Sanches-Vives MV, Nowak LG, McCormick DA (2000a) Membrane mechanisms underlying contrast adaptation in cat area 17 in vivo. Journal of Neuroscience 20: 4267 – 4585.

Sanches-Vives MV, Nowak LG, McCormick DA (2000b) Cellular mechanisms of long-lasting adaptation in visual cortical neurons in vitro. Journal of Neuroscience 20: 4286 – 4299.

Saul AB, Cynader MS (1989a) Adaptation in single units in visual cortex: the tuning of aftereffects in the spatial domain. Visual Neuroscience 2: 593 – 607.

Saul AB, Cynader MS (1989b) Adaptation in single units in visual cortex: the tuning of aftereffects in the temporal domain. Visual Neuroscience 2: 509 – 620.

Sceniak MP, Ringach DL, Hawken MJ, Shapley R. (1999) Contrast's effect on spatial summation by macaque V1 neurons. Nature Neuroscience 2: 733 – 739.

Schall JD, Hanes DP, Thompson KG, D.J. King DJ (1995) Saccade target selection in frontal eye field of macaque. I. Visual and premovement activation. Journal of Neuroscience 15: 6905 – 6918.

Schiller PH, Finlay BL, Volman SF (1976) Quantitative studies of single-cell properties in monkey striate cortex. III. Spatial frequency. Journal of Neurophysiology 39: 1334 – 1351.

Schlack A, Krekelberg, Albright TD (2008) Speed perception during acceleration and deceleration. Journal of Vision 8: 1 – 11.

Schuett S, Bonhoeffer T, Hübener M (2002) Mapping retinotopic structure in mouse visual cortex with optical imaging. Journal of Neuroscience 22: 6549 – 6659.

Sclar G, Freeman RD (1982) Orientation selectivity in the cat's striate cortex is invariant with stimulus contrast. Experimental Brain Research 46: 457 – 461.

Sclar G, Lennie P, DePriest DD (1989) Contrast adaptation in striate cortex of macaque. Vision Research 29: 747 – 755.

Sclar G, Maunsell JH, Lennie P (1990) Coding of image contrast in central visual pathways of the macaque monkey. Vision Research 30: 1 – 10.

Shou T, Li X, Zhou Y, Hu B (1996) Adaptation of visually evoked responses of relay cells in the dorsal lateral geniculate nucleus of the cat following prolonged exposure to drifting gratings. Visual Neuroscience 13: 605 – 613.

Simoncelli EP, Heeger DJ (2001) Representing retinal image speed in visual cortex. Nature Neuroscience 4: 461 – 462.

Sincich LC, Horton JC (2002a) Divided by cytochrome oxidase: a map of the projections from V1 to V2 in macaques. Science 295: 1734 – 1737.

Sincich LC, Horton JC (2002b) Pale cytochrome oxidase stripes in V2 receive the richest projection from macaque striate cortex. Journal of Comparative Neurology 447: 18 – 33.

Sincich LC, Horton JC (2003) Independent projection streams from macaque striate cortex to the second visual area and middle temporal area. Journal of Neuroscience 23: 5684 – 5692.

Skottun BC, De Valois RL, Grosof DH, Movshon JA, Albrecht DG, Bonds AB (1991) Classifying simple and complex cells on the basis of response modulation. Vision Research 31: 1079 – 1086.

Stroud AC, LeDue EE, Crowder NA (2012) Orientation specificity of contrast adaptation in mouse primary visual cortex. Journal of Neurophysiology, In press.

Tian L, Hires SA, Mao T, Huber D, Chiappe ME, Chalasani SH, Petreanu L, Akerboom J, McKinney SA, Schreiter ER, Bargmann CI, Jayaraman V, Svoboda K, Looger LL (2009) Imaging of neural activity in worms, flies and mice with improved GCaMP calcium indicators. Nature Methods 6: 875 – 881.

Tolhurst DJ and Dean DF (1987) Spatial summation of simple cells in the striate cortex of the cat. Experimental Brain Research 66: 607 – 620.

Umino Y, Solessio E, Barlow RB (2008) Speed, spatial, and temporal tuning of rod and cone vision in mouse. Journal of Neuroscience 28: 189 – 198.

Valverde F (1991) The organization of the striate cortex. In: Volume 3, Vision and visual dysfunction. JR Cronly-Dillon ed., London, MacMillan Press.

van Alphen AM, Stahl JS, De Zeeuw CI (2001) The dynamic characteristics of the mouse horizontal vestibule-ocular and optokinetic response. Brain Research 890: 296 – 305.

Van den Bergh G, Zhang B, Arckens L, Chino YM (2010) Receptive-field properties of V1 and V2 neurons in mice and macaque monkeys. Journal of Comparative Neurology 518: 2051 – 2070.

Van Essen DC (1979) Visual areas of the mammalian cerebral cortex. Annual Reviews of Neuroscience 2: 227 – 263.

Wagor E, Mangini NJ, Pearlman AL (1980) Retinotopic organization of striate and extrastriate visual cortex in the mouse. Journal of Comparative Neurology 193: 187 – 202.

Wang Q, Burkhalter A (2007) Area map of mouse visual cortex. Journal of Comparative Neurology 502: 339 – 357.

Wang L, Sarnaik R, Rangarajan K, Liu X, Cang J (2010) Visual receptive field properties of neurons in the superficial superior colliculus of the mouse. Journal of Neuroscience 30: 16573 – 16584.

Wang Q, Sporns O, Burkhalter A (2012) Network analysis of corticocortical connections reveals ventral and dorsal processing streams in mouse visual cortex. Journal of Neuroscience 32: 4386 – 4399.

Wang YV, Weick M, Demb JB (2011) Spectral and temporal sensitivity of cone-mediated responses in mouse retinal ganglion cells. Journal of Neuroscience 31: 7670 – 7681.

Wielaard DJ, Shelley M, McLaughlin D, Shapley R (2001) How simple cells are made in a nonlinear network model of the visual cortex. Journal of Neuroscience 21: 5203 – 5211.

Wikler KC, Rakic P (1990) Distribution of photoreceptor subtypes in the retina of diurnal and nocturnal primates. Journal of Neuroscience 10: 3390 – 3401.

Wikler KC, Williams RW, Rakic P (1990) Photoreceptor mosaic: number and distribution of rods and cones in the rhesus monkey retina. Journal of Comparative Neurology 297: 499 – 508.

Xing D, Ringach DL, Shapley R, Hawken MJ (2004) Correlation of local and global orientation and spatial frequency tuning in macaque V1. Journal of Physiology 557: 923 – 933.

Yu HH, Verma R, Yang Y, Tibballs HA, Lui LL, Reser DH, Rosa MGP (2010) Spatial and temporal frequency tuning in striate cortex: functional uniformity and specializations related to receptive field eccentricity. European Journal of Neuroscience 31: 1043 – 1062.

Zemel RS, Sejnowski TJ (1998) A model for encoding multiple object motions and self-motion in area MST of primate visual cortex. Journal of Neuroscience 18: 531 – 547.

Zhang F, Aravanis AM, Adamantidis A, de Lecea L, Deisseroth K (2007) Circuit-breakers: optical technologies for probing neural signals and systems. Nature Reviews Neuroscience 8: 577 – 581.